SIAM J. Applied Dynamical Systems
Vol. 22, No. 2, pp. 694–729

An Organizing Center of Codimension Four in a Predator-Prey Model with Generalist Predator: From Tristability and Quadristability to Transients in a Nonlinear Environmental Change*

Min Lu†, Jicai Huang‡, and Hao Wang§

Abstract. In this paper, we take the Rosenzweig–MacArthur (RM) model with generalist predator as an example in a constant or changing environment. When the environment is fixed, we provide a more easily verifiable classification, in terms of the coefficients of the system with nilpotent linear part and general higher terms, to determine the types and codimension of nilpotent singularities in a general planar system. Second, by using the existing classification and some algebraic methods, we show that the highest codimension of a nilpotent focus is 4 and the sample RM model with generalist predator can exhibit nilpotent focus bifurcation of codimension 4. Our results indicate that generalist predation can cause not only richer bifurcations and dynamics (such as multitype tristability and quadristability, a figure-eight loop) but also the possible extirpation of prey. When the environment is changing, we study the impact of the rate μ and intensity β of a nonlinear environmental change on dynamics. The key observations on the asymptotic and transient dynamics include (i) transient tracking on unstable steady states or oscillations, and transient-related regime shifts; (ii) slow and fast regime shifts; (iii) regulation of transient dynamics by the environmental change parameters $|\mu|$ and β; (iv) slow negative or fast positive environmental change can delay or even avoid population extirpation.

Key words. nilpotent focus bifurcation of codimension 4, nonlinear environmental change, transient dynamics, regime shifts, quadristability

MSC codes. 34C23, 34D05, 92Bxx

DOI. 10.1137/22M1488466

1. Introduction.

Using the long-term dynamics from bifurcation analysis in a constant environment to understand the response and transient dynamics of populations to environmental fluctuations is a cutting-edge area of ecology. Ecosystems are undergoing environmental changes, such as extreme climate events, land-use change, disease outbreaks, and other environmental perturbations. Understanding and predicting the response of populations to environmental fluctuations is a major challenge in ecology. Mathematical models can provide

* Received by the editors April 4, 2022; accepted for publication (in revised form) by C. Postlethwaite October 9, 2022; published electronically May 31, 2023.
https://doi.org/10.1137/22M1488466
Funding: This research was partially supported by NSFC grants 11871235 and 12231008 and NSERC grants RGPIN-2020-03911 and RGPAS-2020-00090.
† School of Mathematics and Statistics & Hubei Key Laboratory of Mathematical Sciences, Central China Normal University, Wuhan, Hubei 430079, People's Republic of China (lumin@mails.ccnu.edu.cn).
‡ Corresponding author. School of Mathematics and Statistics & Hubei Key Laboratory of Mathematical Sciences, Central China Normal University, Wuhan, Hubei 430079, People's Republic of China (hjc@mail.ccnu.edu.cn).
§ Corresponding author. Department of Mathematical and Statistical Sciences, University of Alberta, Edmonton, Alberta T6G 2G1, Canada (hao8@ualberta.ca).

useful insights into this topic. From the pioneering work of Lotka [23] and Volterra [32] in the 1920s to the seminal one of May [26] in the 1970s, most of the efforts have been focused on the asymptotic behaviors to predict the population persistence or extinction. However, there is an increasing recognition that the asymptotic dynamics may or may not reflect realistic observations (see [19] and references therein). In contrast, transient dynamics, i.e., dynamics on ecological time scales, normally gives us more relevant information about the response of populations to environmental changes. There have been some important reviews and explorations about transients, especially long transients, in ecology (see [19, 27] and references therein), where a classification of transient dynamics and several main mechanisms leading to the emergence of long transients were revealed in different models. However, systems with explicit time dependence (i.e., nonautonomous systems) describing interacting species in a changing environment have not been emphasized in [19, 27] due to the lack of equilibria and great mathematical challenges related to the broader area of the nonequilibrium concept in ecological systems. In the most recent works [3, 4], Arumugam, Guichard, and Lutscher assumed that the prey's carrying capacity is a linear function of time t and used the bifurcation diagrams in a constant environment together with transients to explore the response of populations to linear environmental changes. They found that the species in a changing environment can track unstable states in a constant environment before shifting to stable states. Xiang, Huang, and Wang [34] linked bifurcation analysis of the Holling–Tanner model with generalist predator to a changing environment, and used the asymptotic dynamics from bifurcation analysis in a constant environment to understand and predict the response of populations to environmental fluctuations. Especially, they studied theoretically the response in a periodic environment and found that the populations converge to a periodic solution or an invariant torus depending on the initial environmental capacity and the amplitude of periodic fluctuation. To the best of our knowledge, all existing works focused on linear environmental changes, hence we are the first to explore the impact of nonlinear environmental changes on transient dynamics here.

In order to explore the response and transient dynamics of populations to nonlinear environmental fluctuations, we formulate the following Rosenzweig–MacArthur model with generalist predation and nonlinear environmental change,

$$\begin{aligned} \frac{dN}{dt} &= RN\left(1-\frac{N}{K}\right)-\frac{\alpha NP}{A+N}, \\ \frac{dP}{dt} &= \frac{\gamma NP}{A+N}+\frac{CP}{1+QP}-MP, \\ K(t) &= (K_0+\mu t)^{\beta}, \end{aligned} \tag{1.1}$$

where N and P denote densities of the prey and predator population, respectively, at time t with nonnegative initial conditions $N(0)\geq 0$ and $P(0)\geq 0$. R and K are the intrinsic growth rate and the environmental carrying capacity of the prey, α is the maximum consumption rate of prey by the predator, A is the half-saturation constant, and γ is the conversion efficiency from prey to predator. In the absence of the focal prey N, the predator population grows with a logistic-like function (i.e., a Beverton–Holt-like function) $\frac{CP}{1+QP}-MP$, where M is the mortality rate of the predator, C is the maximum per capita reproduction rate of the predator in the absence of the focal prey, and Q is the strength of density dependence. All parameters are naturally positive. We assume that the predator is a *generalist predator*, which

has several alternative prey species for food and can persist by switching to other food sources even when the focal prey is scarce. Thus we always assume $C > M$. In the third equation of system (1.1), $K_0 > 0$ denotes the initial carrying capacity. $\beta > 0$ represents the intensity of nonlinear environmental change; the larger β is, the stronger the intensity of environmental change. When $\beta = 1$, the rate of environmental change is a linear function; otherwise that is a nonlinear function: convex if $0 < \beta < 1$; concave if $\beta > 1$. μ represents the speed and direction of environmental change; the larger the $|\mu|$, the faster the environmental change. The prey's carrying capacity $K(t)$ increases over time if $\mu > 0$ and decreases if $\mu < 0$.

When $\mu = 0$ and $C = 0$, i.e., the environment does not change and the predator is a *specialist*, system (1.1) becomes the classical Rosenzweig–Macarthur (RM) model [29, 30], whose long-term asymptotic dynamics are well understood. Two boundary equilibria always exist, the coextinction saddle $E_0(0,0)$ and prey-only steady state $E_K(K,0)$, and there exists at most one coexistence steady state E_1. There are two thresholds K_1 and K_2 ($K_1 < K_2$) for the prey's carrying capacity: when $K < K_1$, E_K is globally asymptotically stable and the predator goes extinct for all positive initial densities; when $K = K_1$, a transcritical bifurcation occurs; when $K_1 < K < K_2$, the predator can invade and coexist with the prey, E_K becomes unstable, and E_1 is globally asymptotically stable; when $K = K_2$, a supercritical Hopf bifurcation occurs; when $K > K_2$, E_1 becomes unstable, and a stable and unique periodic oscillation arises. It is worth noting that the prey always persists for all positive initial densities and all admissible parameter values.

When $\mu = 0$ and $C > M$, then the environment does not change and the predator is a *generalist*, and system (1.1) becomes the following RM model with generalist predator [16, 28]:

$$\begin{aligned} \frac{dN}{dt} &= RN\left(1 - \frac{N}{K}\right) - \frac{\alpha NP}{A+N}, \\ \frac{dP}{dt} &= \frac{\gamma NP}{A+N} + \frac{CP}{1+QP} - MP. \end{aligned} \tag{1.2}$$

Sen et al. [28] showed, mainly by numerical simulations, that system (1.2) exhibits rich and complex dynamics like bistability, tristability along with some local and global bifurcations like Bogdanov–Takens bifurcation, homoclinic bifurcation, etc. However, the detailed classification of equilibria, especially the types and codimension of nilpotent singularities and the high codimension bifurcations, were not theoretically analyzed in any work.

There are 8 parameters in system (1.2), and as parameters vary, the dynamics will often change. Thus, in order to understand the local or global dynamics of system (1.2), we need to know which parameters are the main ones to affect the asymptotic dynamics, what are the sensitive values of the main parameters to cause the dynamical changes, and what are the dynamical patterns when the main parameters vary around their sensitive values. These are related to the bifurcation theory of dynamical systems. The main parameters and their sensitive values are called bifurcation parameters and bifurcation values, respectively. If the qualitative structure of a system changes when parameters vary, the vector field at a parameter value where a qualitative change occurs is called structurally unstable. One of the main tasks in bifurcation theory is to deal with so-called universal problems, i.e., finding the versal unfoldings of structurally unstable vector fields. Roughly speaking, finding the versal unfolding is to find a special perturbation system which contains all different dynamics "near" a given structurally unstable vector field. If there exists a versal unfolding, then it is usually not

unique, and the least number of parameters within versal unfoldings is called the codimension of this bifurcation, which can be used to measure the degree of bifurcation complexity. Many bifurcations of system (1.2) have been shown numerically such as local bifurcations: saddle-node bifurcation, Hopf bifurcation, and global bifurcations: homoclinic bifurcation, saddle-node bifurcation of limit cycles. Can we rigorously prove the existence of these bifurcations? How are these bifurcations organized in parameter space? Are there some high codimension bifurcations serving as organizing centers that locally (and often semiglobally) determine the geometry of the bifurcation set? High codimension nilpotent bifurcations can often take the role. In the 8-parameter family of vector field (1.2), the highest codimension of bifurcations is generically not larger than the number 8 of parameters, say m ($m \leq 8$); then the codimension m bifurcations are isolated points in m-dimensional parameter space, from which a series of bifurcations with lower codimension originate. In other words, the bifurcations of codimension less than m are subordinate to one or more codimension m equilibria [9], which act as organizing centers for the bifurcation diagram. For instance, Bogdanov–Takens bifurcation is a codimension 2 bifurcation, which contains a series of codimension 1 bifurcations: saddle-node, Hopf, and homoclinic bifurcations. The codimension 2 cusp serves as the organizing center of the Bogdanov–Takens bifurcation diagram. Recently, some researchers have concentrated on searching for nilpotent bifurcations with highest codimension in many mathematical models (see [1, 2, 5, 8, 9, 10, 22, 24, 25, 33, 35, 40, 42] and reference therein).

In this paper, we will first revisit the asymptotic dynamics of system (1.2) (i.e., system (1.1) in a constant environment) by rigorous bifurcation analysis, especially high codimension nilpotent bifurcations. Next, based on the bifurcation results for system (1.2), we will explore the response of populations to environmental fluctuations for system (1.1) in a changing environment.

In a constant environment, all parameters do not change over time in system (1.2). We will provide a more easily verifiable classification compared with that in [10], in terms of the coefficients of the system with nilpotent linear part and general higher terms, to determine the types and codimension of nilpotent singularities in a general planar system. Based on the previous classification and using some algebraic methods (including resultant elimination [17], Sturm's theorem, complete discrimination system for polynomials [39], and a real root isolation algorithm) to solve the semialgebraic varieties of normal form coefficients, we will provide a complete classification about the types of equilibria for system (1.2), especially the types and codimension of nilpotent singularities, and show that the highest codimension of a nilpotent focus is 4 and system (1.2) can exhibit nilpotent focus bifurcation of codimension 4, which implies that the codimension 4 nilpotent focus serves as the potential organizing center of the bifurcation set. Our results indicate that generalist predation can cause not only richer bifurcations and dynamics, such as multitype tristability, multitype quadristability (two positive equilibria and two big limit cycles; two positive equilibria, one small limit cycle, and one big limit cycle), and figure-eight loop, but also the extirpation of prey for some positive initial densities. To the best of our knowledge, it is the first time that multitype quadristability and nilpotent focus bifurcation of codimension 4 are rigorously shown in a predator-prey system.

In a changing environment, we assume that the habitat quality (i.e., carrying capacity) undergoes a nonlinear environmental change in system (1.1). Due to a general and direct time

dependence and the lack of equilibria in system (1.1) when $\mu \neq 0$, we will study the dynamics of system (1.1) mainly by numerical methods, compare dynamics under environmental change with bifurcation results under constant environment, and predict the response and transient dynamics of populations to nonlinear environmental fluctuations. We will find some important characteristics, such as (i) transient tracking (unstable steady states or oscillations) and transient-related regime shifts (positive stable steady states to oscillations and vice versa; one positive stable steady state to another positive stable steady state; one positive stable steady state to one boundary stable steady state); (ii) slow and fast regime shifts (shifting to stable oscillations slower than to stable steady states); (iii) different values of speed $|\mu|$ or intensity β induce different transient dynamics; (iv) slow negative or fast positive environmental change can delay or avoid population extirpation. To the best of our knowledge, this is the first exploration to consider nonlinear environmental changes in an ecosystem.

The rest of the paper is organized as follows. In section 2, we provide a complete bifurcation analysis, especially nilpotent bifurcations with high codimension, for system (1.2). In section 3, we explore the impact of a nonlinear environmental change on the transient dynamics in system (1.1). A brief summary is given in the last section. Most detailed proofs are presented in the appendices.

2. Constant environment.

In this section, under constant environment $\mu = 0$, we will give a complete bifurcation analysis, especially nilpotent bifurcations with high codimension, for system (1.2).

Before going into details, we rescale system (1.2) by $N = Kx$, $P = \frac{RK}{\alpha} y$, $\frac{dt}{d\tau} = \frac{1}{R}$; then system (1.2) becomes (still denote τ by t)

$$\begin{aligned} \frac{dx}{dt} &= x\left(1 - x - \frac{y}{a+x}\right), \\ \frac{dy}{dt} &= y\left(\frac{bx}{a+x} + \frac{c+m}{1+qy} - m\right), \end{aligned} \tag{2.1}$$

where $a = \frac{A}{K}$, $b = \frac{\gamma}{R}$, $c = \frac{C-M}{R}$, $q = \frac{QRK}{\alpha}$, $m = \frac{M}{R}$, and a, b, c, q, m are all positive parameters.

From the biological point of view, we consider system (2.1) in $\mathbb{R}^2_+ = \{(x, y) \,|\, x \geq 0, y \geq 0\}$. Moreover, it is not difficult to see that

$$\Omega = \left\{(x, y) | \, 0 \leq x \leq 1,\ y \geq 0,\ bx + y \leq b + \frac{qb + c + m}{qm}\right\}$$

is a positive invariant and attracting region for the semiflows of system (2.1) in $\mathbb{R}^2_+$.

2.1. Boundary equilibria and their types.

System (2.1) always has three boundary equilibria $A_1(0,0)$, $A_2(1,0)$, and $A_3(0, \frac{c}{qm})$ for all admissible parameters. By using Theorem 7.1 in chapter 2 of [41], we obtain the following results.

Lemma 2.1. *System (2.1) always has three boundary equilibria $A_1(0,0)$, $A_2(1,0)$, and $A_3(0, \frac{c}{qm})$. Moreover, $A_1(0,0)$ is always a hyperbolic unstable node, $A_2(1,0)$ is always a hyperbolic saddle, and*

(I) *if $c < qma$, then $A_3(0, \frac{c}{qm})$ is a hyperbolic saddle;*
(II) *if $c > qma$, then $A_3(0, \frac{c}{qm})$ is a hyperbolic stable node;*
(III) *if $c = qma$ and*

(i) $b > \frac{(1-a)amq}{1+aq}$, *then* $A_3(0, \frac{c}{qm})$ *is a saddle node of codimension* 1 *which includes a stable parabolic sector in the right half-plane;*

(ii) $b < \frac{(1-a)amq}{1+aq}$ *and* $0 < a < 1$, *then* $A_3(0, \frac{c}{qm})$ *is a saddle-node of codimension* 1 *which includes a stable parabolic sector in the left half-plane;*

(iii) $b = \frac{(1-a)amq}{1+aq}$, *and*

(a) $q > \frac{1-2a}{a^3}$, *then* $A_3(0, \frac{c}{qm})$ *is a stable node of codimension* 2*;*

(b) $q < \frac{1-2a}{a^3}$, *then* $A_3(0, \frac{c}{qm})$ *is a saddle of codimension* 2*;*

(c) $q = \frac{1-2a}{a^3}$, *then* $A_3(0, \frac{c}{qm})$ *is a saddle node of codimension* 3 *which includes a stable parabolic sector in the right half-plane.*

2.2. Nilpotent equilibria and nilpotent bifurcations. In order to study positive equilibria and their types in system (2.1), we first provide some criteria, in terms of the coefficients of the system with nilpotent linear part and general higher terms, to determine the types and codimension of nilpotent equilibria in a general planar system.

Consider a family of planar vector fields

$$\frac{dx}{dt} = F(x, y, \epsilon), \quad \frac{dy}{dt} = G(x, y, \epsilon), \tag{2.2}$$

where $x, y \in \mathbb{R}^1, \epsilon = (\epsilon_1, \epsilon_2, \ldots, \epsilon_m) \in \mathbb{R}^m, m \geq 2$, and $F, G \in C^\infty(x, y, \epsilon)$.

We suppose, for $\epsilon = \epsilon_0$, that $(0,0)$ is a nilpotent equilibrium of system (2.2), and the Jacobian matrix of system $(2.2)|_{\epsilon=\epsilon_0}$ at $(0,0)$ is as follows:

$$J(E) = \begin{pmatrix} 0 & 1 \\ 0 & 0 \end{pmatrix}. \tag{2.3}$$

Then, the Taylor expansion of system $(2.2)|_{\epsilon=\epsilon_0}$ around the origin takes the form

$$\begin{aligned} \dot{x} &= y + \sum_{2 \leq i+j \leq 5} a_{ij} x^i y^j + o(|x, y|^5), \\ \dot{y} &= \sum_{2 \leq i+j \leq 5} b_{ij} x^i y^j + o(|x, y|^5). \end{aligned} \tag{2.4}$$

Let $x = X + \frac{a_{11}+b_{02}}{2} X^2$, $y = Y - a_{20}X^2 + b_{02}XY - a_{02}Y^2$; then system (2.4) becomes

$$\begin{aligned} \dot{x} &= y + \sum_{3 \leq i+j \leq 5} c_{ij} x^i y^j + o(|x, y|^5), \\ \dot{y} &= d_{20}x^2 + d_{11}xy + \sum_{3 \leq i+j \leq 5} d_{ij} x^i y^j + o(|x, y|^5), \end{aligned} \tag{2.5}$$

where c_{ij} and d_{ij}, expressed by a_{ij} and b_{ij}, are given in Appendix I.

(i) If $d_{20}d_{11} \neq 0$ in (2.5), then $(0,0)$ of system $(2.2)|_{\epsilon=\epsilon_0}$ is a nilpotent cusp of codimension 2 (see [6, 7, 31]).

Lemma 2.2. *If* $\epsilon = \epsilon_0$ *and* $d_{20}d_{11} \neq 0$ *given in system* (2.5) *hold, then* $(0,0)$ *of system* (2.2) *is a cusp of codimension* 2 *(i.e., Bogdanov–Takens singularity).*

When $d_{20}d_{11} = 0$, we need the following simpler normal form to classify further the types and codimension of $(0,0)$; the proof is shown in Appendix II.

Lemma 2.3. *For $\epsilon=\epsilon_0$, system (2.5) is locally topologically equivalent to*

$$\begin{aligned}\dot{x}&=y+o(|x,y|^5),\\ \dot{y}&=j_{20}x^2+j_{11}xy+j_{30}x^3+j_{21}x^2y+j_{40}x^4+j_{31}x^3y+j_{50}x^5+j_{41}x^4y+o(|x,y|^5),\end{aligned}\tag{2.6}$$

where j_{ij} can be expressed by c_{ij} and d_{ij}.

(ii) If $d_{11}=0$ and $d_{20}\neq 0$ in (2.5), then $(0,0)$ of system (2.2) is a nilpotent cusp of codimension at least 3 (see [11, 13, 21]). We have the following results; the detailed proof is shown in Appendix II.

Lemma 2.4. *If $\epsilon=\epsilon_0$, $d_{20}\neq 0$, and $d_{11}=0$ given in system (2.5) hold, then system (2.2) is locally topologically equivalent to*

$$\begin{aligned}\dot{x}&=y,\\ \dot{y}&=x^2+\bar{M}x^3y+\bar{N}x^4y+o(|x,y|^5),\end{aligned}\tag{2.7}$$

where $\bar{M}$ and $\bar{N}$, expressed by c_{ij} and d_{ij}, are given in Appendix II.

Moreover, $(0,0)$ of system (2.7) is a codimension 3 cusp if $\bar{M}\neq 0$, a codimension 4 cusp if $\bar{M}=0$ and $\bar{N}\neq 0$, and a cusp of codimension at least 5 if $\bar{M}=0$ and $\bar{N}=0$.

(iii) If $d_{20}=0$ in (2.5), then $(0,0)$ of system (2.2) is a nilpotent saddle (or focus or elliptic singularity) of codimension at least 3 (see [12, 14, 15, 18, 20, 36, 43]). We have the following results; the detailed proof is shown in Appendix II.

Lemma 2.5. *When $\epsilon=\epsilon_0$, $d_{20}=0$, $d_{30}\neq 0$, and $3c_{30}(d_{11}^2+5d_{30})+5d_{21}d_{30}-3d_{11}d_{40}\neq 0$ hold, then system (2.2) is locally topologically equivalent to*

$$\begin{aligned}\dot{x}&=y,\\ \dot{y}&=M_2xy+\epsilon_1x^3+\epsilon_2x^2y+N_2x^3y+o(|x,y|^4),\end{aligned}\tag{2.8}$$

where

$$\epsilon_1=\operatorname{sign}(d_{30}),\quad \epsilon_2=\operatorname{sign}\Big(\frac{3c_{30}(d_{11}^2+5d_{30})+5d_{21}d_{30}-3d_{11}d_{40}}{5d_{30}}\Big),\quad M_2=\frac{d_{11}}{\sqrt{\operatorname{sign}(d_{30})d_{30}}},\tag{2.9}$$

and N_2 is given in Appendix II. Moreover,

(I) *if $d_{11}\neq 0$, the equilibrium $(0,0)$ of system (2.8) is*
- (a) *a nilpotent saddle of codimension 3 if $d_{30}>0$;*
- (b) *a nilpotent focus of codimension 3 if $d_{30}<0$ and $d_{11}^2+8d_{30}<0$;*
- (c) *a nilpotent elliptic equilibrium of codimension 3 if $d_{30}<0$ and $d_{11}^2+8d_{30}>0$;*

(II) *the equilibrium $(0,0)$ of system (2.8) is*
- (a) *a nilpotent saddle of codimension 4 if $d_{30}>0$ and $d_{11}=0$;*
- (b) *a nilpotent focus of codimension 4 if $d_{30}<0$ and $d_{11}=0$;*
- (c) *a nilpotent elliptic equilibrium of codimension at least 4 if $d_{30}<0$ and $d_{11}^2+8d_{30}=0$.*

If $d_{20}=0$, $d_{11}=0$, $d_{30}=0$, $3c_{30}+d_{21}\neq 0$, $d_{40}>0$, and $4c_{40}+d_{31}\neq 0$ in (2.5), then $(0,0)$ of system (2.2) is a nilpotent cusp of codimension 5 [37].

2.3. Positive equilibria and their types. Next, we study the positive equilibria of system (2.1). If $E(x,y)$ is a positive equilibrium of system (2.1), then $y=(1-x)(a+x)$, and x is a real root of the third-order algebraic equation

$$F(x) \triangleq a_3x^3+a_2x^2+a_1x+a_0=0 \tag{2.10}$$

in the interval $(0,1)$, where

$$\begin{aligned} &a_3=q(m-b), \quad a_2=q(a-1)(m-b)+amq,\\ &a_1=b+qa^2m+qa(b-m)+c-amq, \quad a_0=a(c-qam). \end{aligned} \tag{2.11}$$

Let

$$f(x)=\frac{dF(x)}{dx}=3a_3x^2+2a_2x+a_1. \tag{2.12}$$

The Jacobian matrix of system (2.1) at any positive equilibrium $E(x,y)$ takes the form

$$J(E)=\begin{pmatrix} \frac{x(1-a-2x)}{a+x} & -\frac{x}{a+x} \\ \frac{ab(1-x)}{a+x} & -\frac{q(c+m)(1-x)(a+x)}{(1+q(1-x)(a+x))^2} \end{pmatrix}.$$

From $F(x)=0$, we have

$$b=\frac{(a+x)(mq(x-1)(a+x)+c)}{x(aq(x-1)+qx(x-1)-1)};$$

then the determinant $\mathrm{Det}(J(E))$ and $f(x)$ have the following relationship:

$$\mathrm{Det}(J(E))=\frac{(1-x)x}{(a+x)(q(a+x)(1-x)+1)}f(x). \tag{2.13}$$

Thus, the positive equilibrium $E(x,y)$ is an elementary equilibrium if $f(x)\neq 0$, a hyperbolic saddle if $f(x)<0$, and a degenerate equilibrium if $f(x)=0$.

According to the Cardano formula of roots of third-order algebraic equations, we let

$$\hat{A}=a_2^2-3a_1a_3, \quad \hat{B}=27a_3^2a_0-9a_1a_2a_3+2a_2^3, \quad \Delta=\hat{B}^2-4\hat{A}^3; \tag{2.14}$$

then system (2.1) has at most three positive equilibria, denoted by $E_1(x_1,y_1), E_2(x_2,y_2)$, and $E_3(x_3,y_3)$ $(x_1<x_2<x_3)$. Two of them may coalesce into a double positive equilibrium $E_*(x_*,y_*)$, and all of them may coalesce into a unique triple positive equilibrium $E^*(x^*,y^*)$; the number and types of positive equilibria are described in Table 1.

2.3.1. A double positive equilibrium $E_*(x_*,y_*)$. In this subsection, we consider the detailed type of a double positive equilibrium $E_*(x_*,y_*)$ in Table 1, where $y_*=(1-x_*)(a+x_*)$, $0<x_*<1$, $F(x_*)=0$, $F'(x_*)=0$, and $F''(x_*)\neq 0$.

Define

$$\begin{aligned} &b=b_*\triangleq\frac{x_*(1-a-2x_*)^2}{a(1-x_*)}, \quad m=m_*\triangleq\frac{x_*(1-a-2x_*)}{aq(1-x_*)(a+x_*)^2}\Big[a+q(a+x_*)^2(1-2x_*)\Big],\\ &c=c_*\triangleq\frac{x_*(1-a-2x_*)}{a(1-x_*)(a+x_*)}\Big[a+x_*(2x_*-1)+qa(a+x_*)(x_*-1)^2\Big], \end{aligned} \tag{2.15}$$

Table 1

Number and types of positive equilibria in system (2.1). Notation Ⓐs (resp., Ⓢa, Ⓓ) denotes antisaddle (resp., saddle, degenerate).

b	c	Conditions of parameters	Positive equilibrium	
$\geq m$	$< qam$		1	E_2: Ⓐs
	$\geq qam$		0	
$< m$	$= qam$	$a_2^2 - 4a_1a_3 > 0$, $a_1 > 0$ and $a_2 < 0$	2	E_2: Ⓢa E_3: Ⓐs
		$a_2^2 - 4a_1a_3 > 0$, $a_1 = 0$ and $a_2 < 0$	1	E_3: Ⓐs
		$a_2^2 - 4a_1a_3 > 0$ and $a_1 < 0$	1	E_3: Ⓐs
		$a_2^2 - 4a_1a_3 = 0$, $a_1 > 0$ and $a_2 < 0$	1	E_*: Ⓓ
		$a_2^2 - 4a_1a_3 < 0$ $a_2^2 - 4a_1a_3 = 0$, $a_1 \geq 0$ and $a_2 \geq 0$ $a_2^2 - 4a_1a_3 > 0$, $a_1 \geq 0$ and $a_2 > 0$	0	
	$> qam$	$\Delta < 0$, $a_2 < \sqrt{\hat{A}} < 3a_3 + a_2$	2	E_2: Ⓢa E_3: Ⓐs
		$\Delta = 0$ and $\max\{0, a_2\} < \sqrt{\hat{A}} < 3a_3 + a_2$	1	E_*: Ⓓ
		$\Delta > 0$ $\Delta = 0$ and $\hat{A} = 0$ $\Delta \leq 0$ and $0 < \sqrt{\hat{A}} < a_2$ $\Delta \leq 0$ and $\sqrt{\hat{A}} > \max\{0, 3a_3 + a_2\}$	0	
	$< qam$	$\Delta < 0$, $\sqrt{\hat{A}} < -a_2$	3	E_1 and E_3: Ⓐs E_2: Ⓢa
		$\Delta = 0$, $0 < \sqrt{\hat{A}} < -a_2$ and $B = 2A^{\frac{3}{2}}$	2	E_1: Ⓐs E_*: Ⓓ
		$\Delta = 0$, $0 < \sqrt{\hat{A}} < -a_2$ and $B = -2A^{\frac{3}{2}}$	2	E_*: Ⓓ E_3: Ⓐs
		$\Delta = 0$ and $\hat{A} = 0$	1	E^*: Ⓓ
		$\Delta > 0$ $\Delta \leq 0$ and $\sqrt{\hat{A}} > -a_2$	1	E_1(or E_3): Ⓐs

which come from $F(x_*) = 0$, $F'(x_*) = 0$, and $\mathrm{Tr}(J(E_*)) = 0$. Then

$$F''(x_*) = \frac{2x_*(1 - a - 2x_*)(-1 + 2a + 3x_* + q(a + x_*)^3)}{(1 - x_*)(a + x_*)^2}.$$

Let

$$q_1 = \frac{1 - 2a - 3x_*}{(a + x_*)^3}, \quad q_2 = \frac{x_*(1 - 2x_*) - a}{a(1 - x_*)^2(a + x_*)}, \tag{2.16}$$

where $q = q_1$ and $q = q_2$ come from $F''(x^*) = 0$ and $c_* = 0$, respectively. Then from the positivity of b_*, m_*, c_*, and $F''(x_*) \neq 0$, we have the following range about parameters x_*, a, and q:

$$\Omega_1 = \left\{(x_*, a, q) \,|\, 0 < x_* < \frac{1}{2},\ 0 < a < 1 - 2x_*,\ \max\{0, q_2\} < q \neq q_1\right\}.$$

Moreover, define

$$q_* = \frac{a^2 - a(1 - 3x_*) + x_*(1 - 2x_* + 2x_*^2)}{(1 - x_*)(a + x_*)^2(1 - 6x_* + 6x_*^2 - a(1 - 2x_*))}; \tag{2.17}$$

then we have the following results. The detailed proof is given in Appendix III.

Theorem 2.6. *If $(x_*, a, q) \in \Omega_1$ and the conditions in (2.15) hold, then system (2.1) has a double positive equilibrium $E_*(x_*, y_*)$. Moreover, E_* is a cusp of codimension 2 if $q \neq q_*$; otherwise, it is a cusp of codimension 3.*

2.3.2. One triple positive equilibrium $E^*(x^*, y^*)$. In this subsection, we consider the detailed type of the triple positive equilibrium $E^*(x^*, y^*)$ in Table 1, where $y^* = (1-x^*)(a+x^*)$, $F(x^*) = 0$, $F'(x^*) = 0$, and $F''(x^*) = 0$.

From $F(x^*) = 0$, $F'(x^*) = 0$, and $F''(x^*) = 0$, we can express c, m, and q by a, b, and x^* as

$$c = c^* \triangleq \frac{b(-a^2 - 3ax^* + a - x^{*3})}{(a+x^*)^3}, \quad m = m^* \triangleq \frac{b(1-a-3x^*)}{1-2a-3x^*}, \quad q = q^* \triangleq \frac{1-2a-3x^*}{(a+x^*)^3}, \tag{2.18}$$

and $c^*, m^*, q^* > 0$ imply

$$0 < x^* < \frac{1}{4}, \quad a^{1*} < a < a^{2*}, \tag{2.19}$$

where

$$a^{1*} = \frac{1-3x^* - (1-x^*)\sqrt{1-4x^*}}{2} > 0, \quad a^{2*} = \frac{1-3x^*}{2} > 0. \tag{2.20}$$

Moreover, define

$$b^* = \frac{x^*(1-a-2x^*)^2}{a(1-x^*)}, \quad a_1^* = 1 - 6x^* + 4x^{*2}, \quad a_2^* = a_1^* - 2\sqrt{2}(1-x^*)x^*, \tag{2.21}$$

where $b = b^*$ comes from $\mathrm{Tr}(J(E^*)) = 0$; then we have the following results. The detailed proof is given in Appendix IV.

Theorem 2.7. *If the conditions in (2.18) and (2.19) hold, then system (2.1) has a unique positive equilibrium $E^*(x^*, y^*)$, which is an unstable (or a stable) degenerate node if $0 < b < b^*$ (or $b > b^*$). Moreover, if $b = b^*$, then E^* is (see Table 2)*

(I) *a nilpotent focus of codimension 3 if one of the following conditions holds:*
  (i) $x^* = \frac{1}{8}$ *or* $\frac{3}{16} \le x^* < \frac{1}{4}$;
  (ii) $\frac{1}{8} < x^* < \frac{3}{16}$ *and* $a \neq a_1^*$;
  (iii) $\frac{2-\sqrt{2}}{8} < x^* < \frac{1}{8}$ *and* $a > a_2^*$;

(II) *a nilpotent elliptic of codimension 3 if* $0 < x^* \le \frac{2-\sqrt{2}}{8}$, *or* $\frac{2-\sqrt{2}}{8} < x^* < \frac{1}{8}$ *and* $a < a_2^*$;

(III) *a nilpotent focus of codimension 4 if* $a = a_1^*$ *and* $\frac{1}{8} < x^* < \frac{3}{16}$;

(IV) *a nilpotent elliptic of codimension 4 if* $a = a_2^*$ *and* $\frac{2-\sqrt{2}}{8} < x^* < \frac{1}{8}$.

2.4. Bifurcations of system (2.1). From Theorem 2.6, we know that system (2.1) may exhibit a degenerate Bogdanov–Takens bifurcation of codimension 3 around the double positive equilibrium E_*. From Theorem 2.7, we can see that system (2.1) may exhibit nilpotent focus or elliptic bifurcations of codimension 3 or 4 around the triple positive equilibrium E^*.

Table 2
Types of a triple positive equilibrium E^* of system (2.1).

x^*	a	d_{30}	d_{11}	$d_{11}^2+8d_{30}$	Types
$[\frac{3}{16},\frac{1}{4})$	(a^{1*}, a^{2*})	<0	<0	<0	Nilpotent focus of codimension 3
$(\frac{1}{8},\frac{3}{16})$	(a_1^*, a^{2*})	<0	<0	<0	Nilpotent focus of codimension 3
	a_1^*	<0	$=0$	<0	Nilpotent focus of codimension 4
	(a^{1*}, a_1^*)	<0	>0	<0	Nilpotent focus of codimension 3
$\frac{1}{8}$	(a^{1*}, a^{2*})	<0	>0	<0	Nilpotent focus of codimension 3
$(\frac{2-\sqrt{2}}{8},\frac{1}{8})$	(a_2^*, a^{2*})	<0	>0	<0	Nilpotent focus of codimension 3
	a_2^*	<0	>0	$=0$	Nilpotent elliptic of codimension 4
	(a^{1*}, a_2^*)	<0	>0	>0	Nilpotent elliptic of codimension 3
$(0,\frac{2-\sqrt{2}}{8}]$	(a^{1*}, a^{2*})	<0	>0	>0	Nilpotent elliptic of codimension 3

The degenerate Bogdanov–Takens bifurcation of codimension 3, nilpotent focus, or elliptic bifurcation of codimension 3 can be shown according to [2, 10, 24, 33, 38, 42]. Thus, we only investigate rigorously if the nilpotent focus bifurcation of codimension 4 can be fully unfolded inside the class of system (2.1).

2.4.1. Nilpotent focus bifurcation of codimension 4. From Theorem 2.7, we know that the unique positive equilibrium $E^*(x^*,y^*)$ of system (2.1) is a nilpotent focus of codimension 4 if $c=c^*$, $m=m^*$, $q=q^*$, $b=b^*$, $a=a_1^*$, and $\frac{1}{8}<x^*<\frac{3}{16}$, where c^*, m^*, q^*, b^*, a_1^* are given in (2.18) and (2.21). Next we show that a nilpotent focus bifurcation of codimension 4 can be fully unfolded inside the class of system (2.1) as (c,m,b,a) vary in the small neighborhood of (c^*,m^*,b^*,a_1^*), i.e., we next show that the unfolding system

$$\begin{aligned}\frac{dx}{dt}&=x\left(1-x-\frac{y}{a_1^*+\lambda_4+x}\right),\\ \frac{dy}{dt}&=y\Big[\frac{(b^*+\lambda_3)x}{a_1^*+\lambda_4+x}+\frac{c^*+\lambda_1+m^*+\lambda_2}{1+q^*y}-(m^*+\lambda_2)\Big],\end{aligned}\tag{2.22}$$

where $\lambda=(\lambda_1,\lambda_2,\lambda_3,\lambda_4)\sim(0,0,0,0)$, can be transformed into the following form:

$$\begin{aligned}\frac{dx}{dt}&=y,\\ \frac{dy}{dt}&=\mu_1(\lambda)+\mu_2(\lambda)x+\mu_3(\lambda)y+\mu_4(\lambda)xy-x^3-x^2y+R(x,y,\lambda),\end{aligned}\tag{2.23}$$

where $R(x,y,\lambda)=O(|x,y|^4)+O(\lambda)(O(y^2)+O(|x,y|^3))+O(\lambda^2)O(|x,y|)$ and $|\frac{\partial(\mu_1,\mu_2,\mu_3,\mu_4)}{\partial(\lambda_1,\lambda_2,\lambda_3,\lambda_4)}|_{\lambda=0}\neq 0$.

It is worth noting that Dangelmayr and Guckenheimer [18] and Khibnik, Krauskopf, and Rousseau [20] partially studied the 4-parameter generic unfolding of codimension 4 nilpotent focus, which was called a doubly degenerate Bogdanov–Takens point in [20]. Here, according to [12, 41], we call it a nilpotent focus of codimension 4. According to [18, 20], we have the following results about system (2.1); the detailed proofs are given in Appendix V.

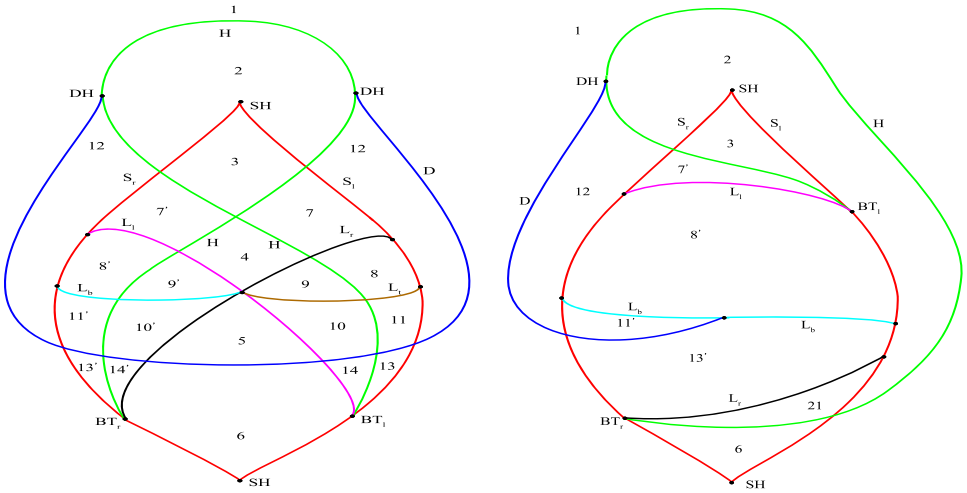

Figure 2.1. (a) *Bifurcation diagram of system* (2.23) *when* $\mu_4 = 0$*;* (b) *bifurcation diagram of system* (2.23) *when* $\mu_4 \gg 0$.

Theorem 2.8. *When* $q = q^*$ *and* $\frac{1}{8} < x^* < \frac{3}{16}$*, system* (2.1) *undergoes a nilpotent focus bifurcation of codimension* 4 *around* E^* *as* (c, m, b, a) *vary in the small neighborhood of* (c^*, m^*, b^*, a_1^*)*, where* c^**,* m^**,* b^**,* a_1^* *are given in* (2.18) *and* (2.21).

Dangelmayr and Guckenheimer [18] and Khibnik, Krauskipt, and Rousseau [20] partially studied the 4-parameter generic unfolding of codimension 4 nilpotent focus. Although there are still some conjectures remaining open, Khibnik, Krauskopf, and Rousseau provided 12 two-dimensional bifurcation diagrams (slices) in Figures 4–5 and 21 structurally stable phase portraits in Figures 1 and 5 in [20] by varying μ_4 from $\mu_4 = 0$ to μ_4 sufficiently large in system (2.23). Moreover, they conjectured the unfolding in $(\mu_1, \mu_2, \mu_3, \mu_4)$-space of (2.23) is given by the transition of the bifurcation set in hyperplanes $\mu_4 = h$ from $h = 0$ to h (sufficiently) large, and it has a conic structure for small values of the parameters.

We plot two of a series of bifurcation sets for system (2.23) in hyperplanes $\mu_4 = 0$ and μ_4 sufficiently large in Figures 2.1(a) and (b), respectively; the 21 structurally stable phase portraits are given in Figure 2.2, where red (resp., blue) dots represent stable (resp., unstable) equilibria, and red (resp., blue) color curves denote stable (resp., unstable) limit cycles (see [20]).

2.4.2. Numerical bifurcation diagrams and phase portraits. In this subsection, we numerically show several biparametric bifurcation diagrams (slices) of system (2.22) (i.e., system (2.1)) by using the Matcont program, and plot phase portraits by choosing different parameter values in the subregion of the bifurcation diagram to illustrate the theoretical results about nilpotent focus bifurcation of codimension 4.

For system (2.22), we take $(c^*, m^*, q^*, b^*, a_1^*) = (\frac{625}{1107}, \frac{11875}{20992}, \frac{131072}{19683}, \frac{3375}{10496}, \frac{41}{256})$, under which system (2.22) has a unique positive equilibrium $E^*(\frac{5}{32}, \frac{2187}{8192})$ which is a nilpotent focus of codimension 4 when $(\lambda_1, \lambda_2, \lambda_3, \lambda_4) = (0, 0, 0, 0)$. Notice that there are always three unstable

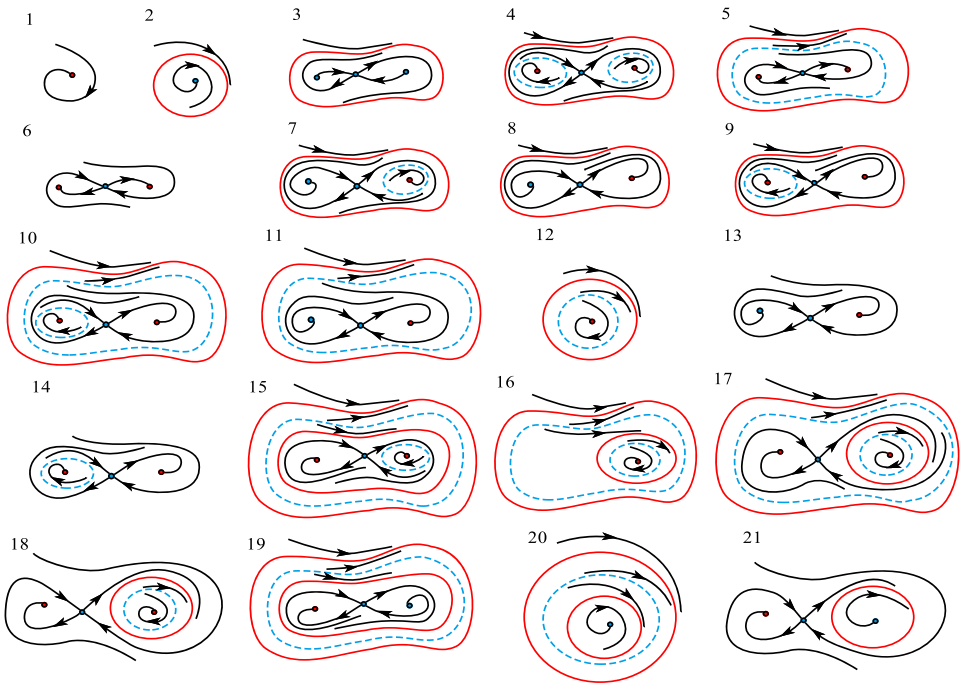

Figure 2.2. *The* 21 *phase portraits appearing in the transition between Figures* 2.1(a) *and* (b).

boundary equilibria $A_1(0,0)$, $A_2(1,0)$, and $A_3(0, \frac{c^*+\lambda_1}{q^*(m^*+\lambda_2)})$ and at most three different positive equilibria $E_1(x_1,y_1)$, $E_2(x_2,y_2)$, $E_3(x_3,y_3)$ $(x_1 < x_2 < x_3)$ of system (2.22). We give the corresponding biparametric bifurcation diagrams in the (λ_4,λ_3) plane with different $\lambda_1's$ and $\lambda_2's$; the bifurcation curves divide the (λ_4,λ_3) plane into several regions; system (2.22) will undergo a series of bifurcations and exhibit abundant dynamics when parameters vary in these regions. Notice that there is always a transcritical bifurcation curve $\lambda_4 = \frac{c^*+\lambda_1}{q^*(m^*+\lambda_2)} - a_1^*$ in the (λ_4,λ_3) plane, which is parallel to the vertical axis. A_3 changes from a saddle to a stable node and E_1 disappears when parameter λ_4 decreases and crosses the transcritical bifurcation curve.

In Figures 2.3(a)–(b) (resp., Figures 2.3(c)–(d)), we give biparametric bifurcation diagrams of system (2.22) in the (λ_4,λ_3) plane with $(\lambda_1,\lambda_2) = (-0.5,-0.1)$ (resp., $(\lambda_1,\lambda_2) = (-0.1,-0.1)$). CP denotes the cusp point, at which the three positive equilibria $E_i\,(i=1,2,3)$ coincide. BT_i $(i = \mathrm{l,r})$ denotes the Bogdanov–Takens bifurcation point, where $\mathrm{BT_l}$ (resp., $\mathrm{BT_r}$) corresponds to the Bogdanov–Takens bifurcation which begins at E_1 and E_2 (resp., E_2 and E_3). GH_i $(i=1,2)$ represents the degenerate Hopf bifurcation point. The saddle-node bifurcation curve SN (the red solid curve) can be divided into two parts by the cusp point CP: the lower part corresponds to the appearance or disappearance of E_1 and E_2 and the upper part corresponds to the appearance or disappearance of E_2 and E_3. The Hopf bifurcation curve H (the green solid curve) tangentially meets the saddle-node bifurcation curve at two points $\mathrm{BT_l}$ and $\mathrm{BT_r}$. The bifurcation curve of the saddle-node bifurcation of limit cycles (the solid blue curve) begins at $\mathrm{GH_1}$. The homoclinic bifurcations $\mathrm{L_l}$ (the magenta dashed curve), $\mathrm{L_r}$ (the black dashed curve), $\mathrm{L_b}$ (the cyan dashed curve), and $\mathrm{L_t}$ (the brown dashed curve)

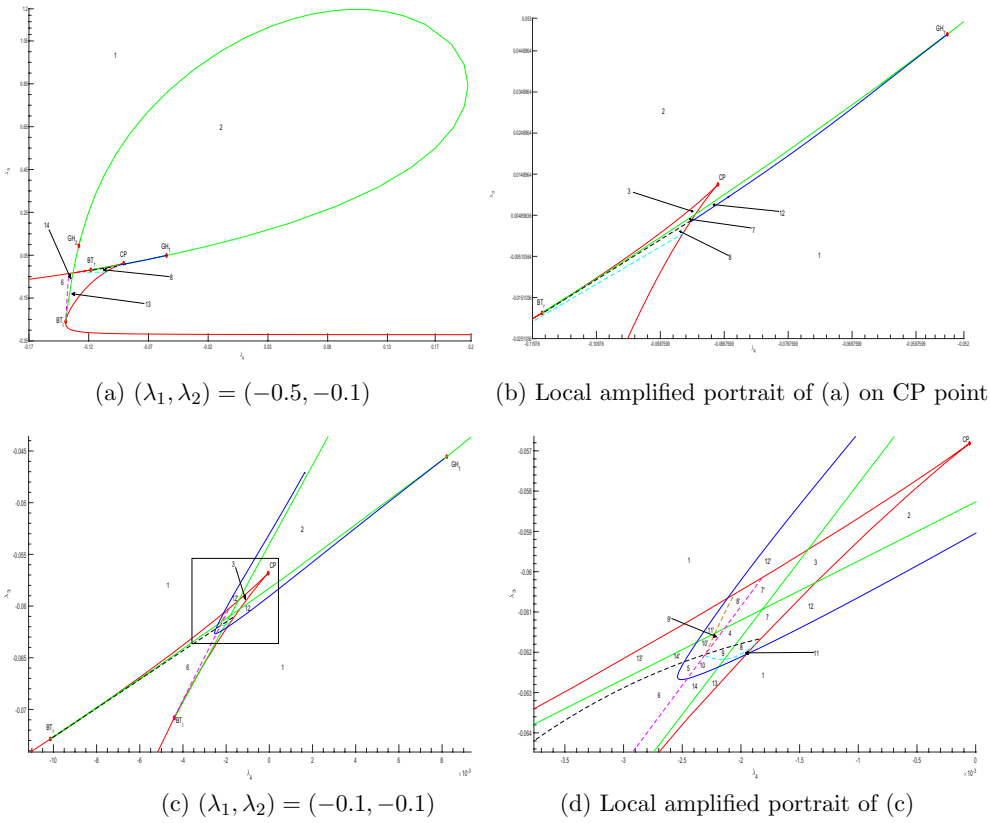

(a) $(\lambda_1, \lambda_2) = (-0.5, -0.1)$ (b) Local amplified portrait of (a) on CP point

(c) $(\lambda_1, \lambda_2) = (-0.1, -0.1)$ (d) Local amplified portrait of (c)

Figure 2.3. *Bifurcation diagram of system* (2.22) *in* (λ_4, λ_3) *plane with* $(c^*, m^*, q^*, b^*, a_1^*) = (\frac{625}{1107}, \frac{11875}{20992}, \frac{131072}{19683}, \frac{3375}{10496}, \frac{41}{256})$ *and different* λ_1 *and* λ_2. BT_i $(i = l,r)$, GH_i $(i = 1, 2)$, *and CP denote respectively Bogdanov–Takens bifurcation point, degenerate Hopf bifurcation point, and cusp point. The red, green, and blue solid curves denote respectively saddle-node bifurcation SN, Hopf bifurcation H, and saddle-node bifurcation of limit cycles. The magenta, black, cyan, and brown dashed curves denote homoclinic bifurcations* $\mathrm{L_l}$, $\mathrm{L_r}$, $\mathrm{L_b}$, *and* $\mathrm{L_t}$, *respectively.*

correspond to a hyperbolic saddle with a homoclinic connection connecting from the left, right, below, and top of the hyperbolic saddle to itself, respectively. The bifurcation curves above divide the (λ_4, λ_3)-plane into 14 regions.

Table 3 shows the detailed dynamical behaviors of system (2.22) in the subregions 1–14 of Figure 2.3. Adding or removing a prime corresponds to a rotation of the phase portrait by π. In Figure 2.4 (resp., Figure 2.5), the corresponding phase portraits for system (2.22) when $(\lambda_1, \lambda_2) = (-0.5, -0.1)$ (resp., $(\lambda_1, \lambda_2) = (-0.1, -0.1)$) and (λ_4, λ_3) located in different regions of Figures 2.3(a) and (b) (resp., Figures 2.3(c) and (d)) are given.

3. Changing environment.

In this section, we let $K(t) = (K_0 + \mu t)^\beta$ and study the effect of the rate μ and intensity β of nonlinear environmental change on the dynamics of system (1.1).

Since system (1.1) does not have any equilibrium if $\mu \neq 0$, we study the effect by numerical simulations. We first use the bifurcation software Matcont to plot one-parameter bifurcation

Table 3

The dynamic behaviors of system (2.22) in different subregions of Figure 2.3. Notation Ⓢ (resp., Ⓤ) represents stable (resp., unstable) positive equilibrium or limit cycle.

Region: phase portrait	Equilibrium	Limit cycle			
		Number	Big	Left	Right
1: Figure 2.4(a)	E_3: Ⓢ	0			
2: Figure 2.4(b)	E_3: Ⓤ	1	Ⓢ		
12: Figure 2.4(c)	E_3: Ⓢ	2	outer: Ⓢ inner: Ⓤ		
3: Figure 2.4(d)	E_1: Ⓤ E_2: Ⓤ E_3: Ⓤ	1	Ⓢ		
4: Figure 2.5(a)	E_1: Ⓢ E_2: Ⓤ E_3: Ⓢ	3	Ⓢ	Ⓤ	Ⓤ
5: Figure 2.5(b)	E_1: Ⓢ E_2: Ⓤ E_3: Ⓢ	2	outer: Ⓢ inner: Ⓤ		
6: Figure 2.5(c)	E_1: Ⓢ E_2: Ⓤ E_3: Ⓢ	0			
7: Figure 2.4(e)	E_1: Ⓤ E_2: Ⓤ E_3: Ⓢ	2	Ⓢ		Ⓤ
8: Figure 2.4(f)	E_1: Ⓤ E_2: Ⓤ E_3: Ⓢ	1	Ⓢ		
9: Figure 2.5(d)	E_1: Ⓢ E_2: Ⓤ E_3: Ⓢ	2	Ⓢ	Ⓤ	
10: Figure 2.5(e)	E_1: Ⓢ E_2: Ⓤ E_3: Ⓢ	3	outer: Ⓢ inner: Ⓤ	Ⓤ	
11: Figure 2.5(f)	E_1: Ⓤ E_2: Ⓤ E_3: Ⓢ	2	outer: Ⓢ inner: Ⓤ		
13: Figure 2.4(g)	E_1: Ⓤ E_2: Ⓤ E_3: Ⓢ	0			
14: Figure 2.4(h)	E_1: Ⓢ E_2: Ⓤ E_3: Ⓢ	1		Ⓤ	

diagrams in the K-P plane (or K-N-P space) for system (1.2) (constant environment); then we plot and include some "representative" trajectories ("time series" or projection of integral curves) of system (1.1) (changing environment) into the bifurcation diagrams. The stable and unstable steady states (or small oscillations) for system (1.2) are denoted, respectively, by solid and dashed curves, and the maximum and minimum values of stable and unstable big oscillations are indicated by black filled and open circles, respectively.

According to the bifurcations and dynamics of system (1.2) given in the previous sections, we focus on the following three interesting bifurcation diagrams (Figures 3.1, 3.2, and 3.8).

The bifurcation diagram in Figure 3.1 shows that system (1.2) undergoes successively supercritical Hopf bifurcation (H_1), subcritical Hopf bifurcation (H_2), and saddle-node bifurcation of limit cycles (LPC) as K increases. The dynamical behaviors of system (1.2) correspond to those in regions 1, 2, 12, 1 of Figure 2.3 as K increases (see Table 3). In this case, three boundary equilibria $A_1(0,0)$, $A_2(K,0)$, and $A_3(0,\frac{C-M}{QM})$ are always unstable. Therefore, system (1.2) exhibits monostability (a stable equilibrium before H_1 or after LPC, a stable oscillation between H_1 and H_2) and bistability (a stable equilibrium and a stable oscillation between H_2 and LPC).

In Figure 3.2, system (1.2) undergoes successively saddle-node bifurcation LP_1, saddle-node bifurcation of limit cycles L_t, homoclinic bifurcation L_t, and subcritical Hopf bifurcation H_1, homoclinic bifurcations L_l, L_r, L_b, saddle-node bifurcation of limit cycles LPC_2, and subcritical Hopf bifurcation H_2 as K increases. The dynamical behaviors of system (1.2) correspond to those in regions 1, 13', 11', 8', 9', 4, 9, 10, 14, 13, 1 of Figure 2.3 (see Table 3). Moreover, three boundary equilibria $A_1(0,0)$, $A_2(K,0)$, and $A_3(0,\frac{C-M}{QM})$ are always unstable. Therefore, system (1.2) exhibits monostability (a stable equilibrium before LP_1 or after LP_2), bistability (a stable equilibrium and a stable big oscillation between L_t and H_1, two stable equilibria between LPC_2 and H_2), and tristability (two stable equilibria and a stable big oscillation between H_1 and LPC_2).

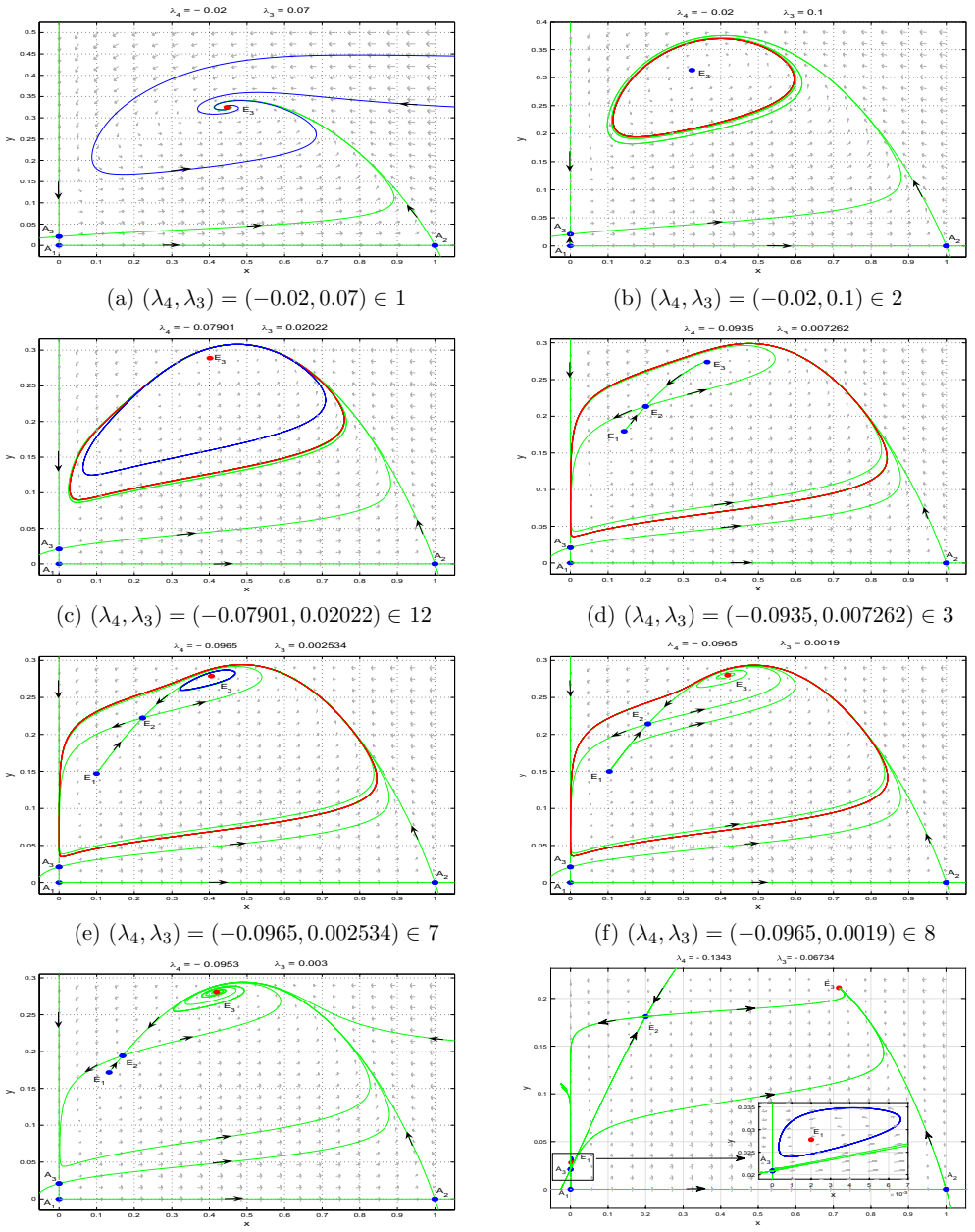

(a) $(\lambda_4, \lambda_3) = (-0.02, 0.07) \in 1$ (b) $(\lambda_4, \lambda_3) = (-0.02, 0.1) \in 2$

(c) $(\lambda_4, \lambda_3) = (-0.07901, 0.02022) \in 12$ (d) $(\lambda_4, \lambda_3) = (-0.0935, 0.007262) \in 3$

(e) $(\lambda_4, \lambda_3) = (-0.0965, 0.002534) \in 7$ (f) $(\lambda_4, \lambda_3) = (-0.0965, 0.0019) \in 8$

(g) $(\lambda_4, \lambda_3) = (-0.0953, 0.003) \in 13$ (h) $(\lambda_4, \lambda_3) = (-0.1343, -0.06734) \in 14$

Figure 2.4. *Phase portraits of system* (2.22) *with* $(c^*, m^*, q^*, b^*, a_1^*) = (\frac{625}{1107}, \frac{11875}{20992}, \frac{131072}{19683}, \frac{3375}{10496}, \frac{41}{256})$, $(\lambda_1, \lambda_2) = (-0.5, -0.1)$, *and* (λ_4, λ_3) *located in different regions of Figures* 2.3(a) *and* (b). *Red (resp., blue) dots represent stable (resp., unstable) equilibria, and red (resp., blue) color curves denote stable (resp., unstable) limit cycles. The detailed dynamical behaviors are described in Table* 3.

A one-parameter bifurcation diagram (black curves) in the K-N-P plane for system (1.2) is given in Figure 3.8. In this case, there exist three boundary equilibria: $A_1(0, 0)$ and $A_2(K, 0)$ are unstable, and $A_3(0, \frac{C-M}{QM})$ is stable. System (1.2) undergoes saddle-node bifurcation at

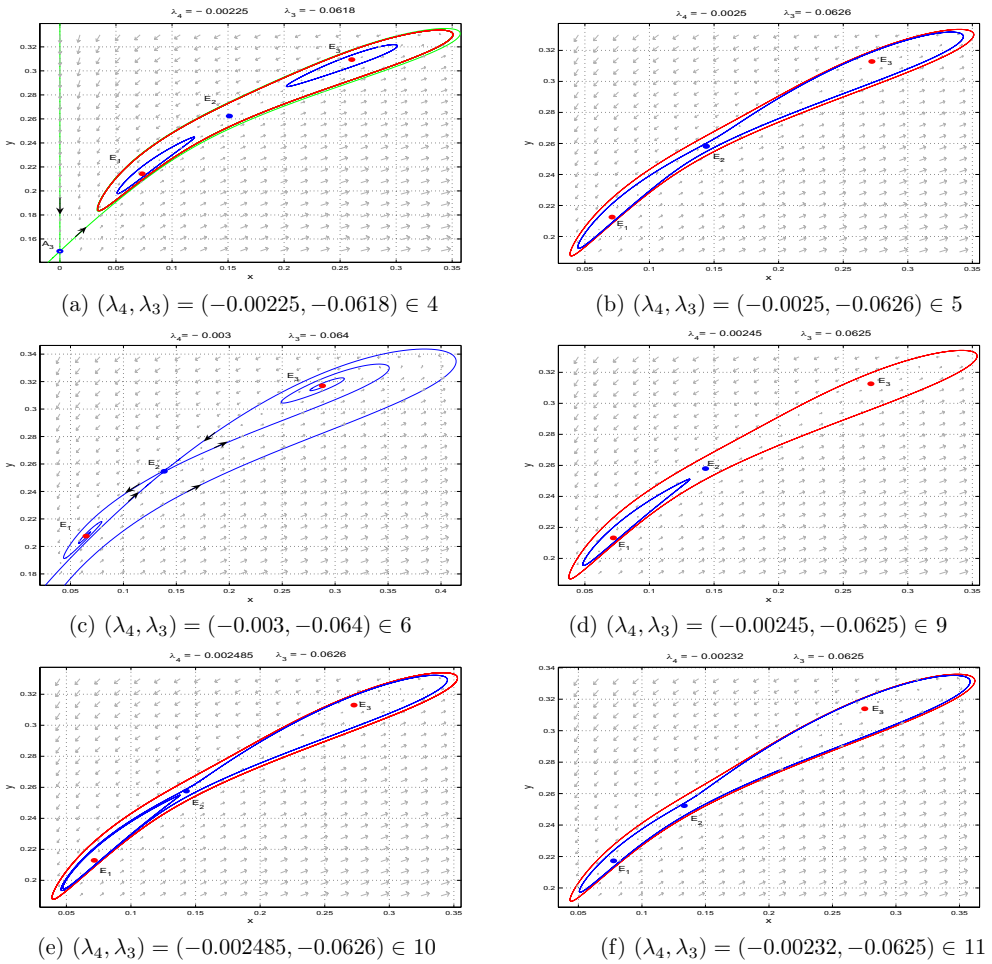

(a) $(\lambda_4, \lambda_3) = (-0.00225, -0.0618) \in 4$

(b) $(\lambda_4, \lambda_3) = (-0.0025, -0.0626) \in 5$

(c) $(\lambda_4, \lambda_3) = (-0.003, -0.064) \in 6$

(d) $(\lambda_4, \lambda_3) = (-0.00245, -0.0625) \in 9$

(e) $(\lambda_4, \lambda_3) = (-0.002485, -0.0626) \in 10$

(f) $(\lambda_4, \lambda_3) = (-0.00232, -0.0625) \in 11$

Figure 2.5. *Phase portraits of system* (2.22) *with* $(c^*, m^*, q^*, b^*, a_1^*) = (\frac{625}{1107}, \frac{11875}{20992}, \frac{131072}{19683}, \frac{3375}{10496}, \frac{41}{256})$, $(\lambda_1, \lambda_2) = (-0.1, -0.1)$, *and* (λ_4, λ_3) *located in different regions of Figures* 2.3(c) *and* (d).

$K = K_{\mathrm{LP}}$, the predator-only steady state $A_3(0, \frac{C-M}{QM})$ is globally stable, and the prey undergoes extinction when $K < K_{\mathrm{LP}}$. (System (2.1) has no positive equilibrium if $K < K_{LP}$, and has a positive invariant, attracting, and bounded region Ω. Thus, A_3 is globally stable if $K < K_{LP}$ since the other two boundary equilibria $A_1(0,0)$ and $A_2(1,0)$ are unstable.) Two positive equilibria occur as $K > K_{\mathrm{LP}}$.

Comparing some representative trajectories (or projections of the integral curves) of system (1.1) with the asymptotic behaviors of system (1.2) predicted by bifurcation diagrams, we observe multiple important characteristics of the asymptotic behaviors and transient dynamics of system (1.1) with environmental changes, such as (a) tracking unstable steady states; (b) slow and fast regime shifts; (c) rate ($|\mu|$) or intensity (β) induced different transient dynamics; (d) tracking unstable oscillations; and (e) delay or avoid (evade) extinctions.

Tracking unstable steady states. When we choose $\mu > 0$ and initial densities near the stable steady state in Figures 3.3(a), (c), (e), we observe that the solution of system (1.1)

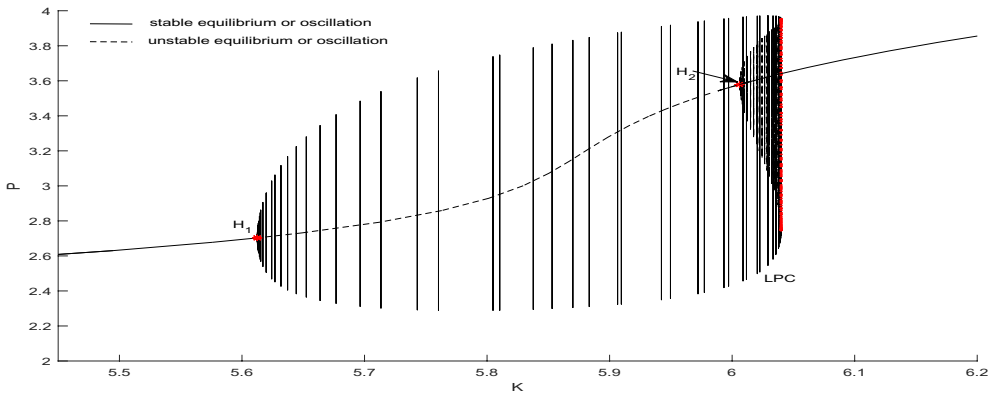

Figure 3.1. *Bifurcation diagram in K-P plane for system (1.2).* H_1, H_2, *and LPC denote supercritical Hopf bifurcation, subcritical Hopf bifurcation, and saddle-node bifurcation of limit cycles, respectively, where* $A=1$, $\gamma=\frac{1}{2}$, $\alpha=1$, $R=\frac{3280000}{1703967}$, $M=\frac{2036625}{2271956}$, $C=\frac{329542625}{184028436}$, $Q=\frac{2271956}{4100625}$.

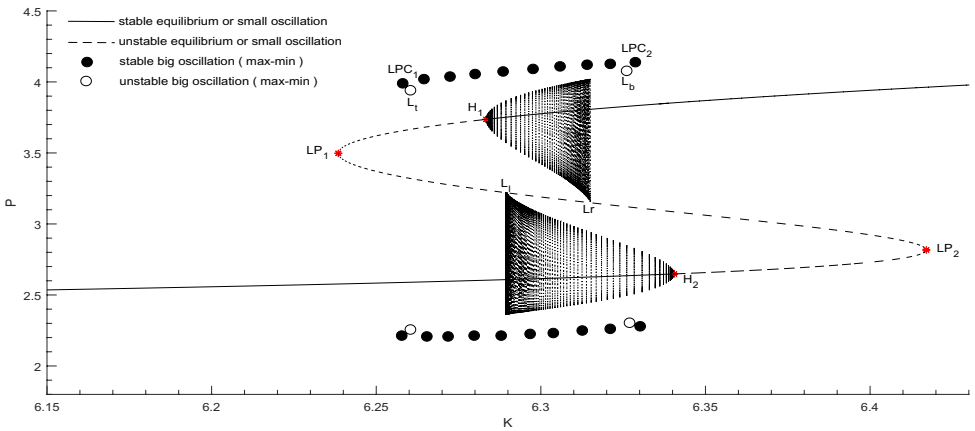

Figure 3.2. *Bifurcation diagram in K-P plane for system (1.2).* $LP_1(LP_2)$, $L_t(LPC_2)$, $L_t(L_l, L_r, L_b)$, $H_1(H_2)$ *denote saddle-node bifurcation, saddle-node bifurcation of limit cycles, homoclinic bifurcations, subcritical Hopf bifurcation, respectively, where* $A=1$, $\gamma=\frac{1}{2}$, $\alpha=1$, $R=\frac{3280000}{1698063}$, $M=\frac{2036625}{2264084}$, $C=\frac{329542625}{183390804}$, $Q=\frac{57147744244}{105078515625}$.

tracks the unstable coexistence steady state after Hopf bifurcation H_1, then switches to the stable oscillation, and takes some time after LPC before it switches to the stable coexistence steady state. Similarly, when $\mu<0$ in Figures 3.3(b), (d), (f), the solution of system (1.1) tracks the unstable coexistence steady state after Hopf bifurcation H_2 before it switches to the stable oscillation, and takes some time after H_1 before it switches to the stable coexistence steady state. Moreover, the tracking appears to last longer for the same β and the higher value of $|\mu|$, where populations switch to the stable oscillations or stable state only when K is much larger ($\mu>0$) or much smaller ($\mu<0$). From Figures 3.3(a), (c), (e) or Figures 3.3(b), (d), (f), we can see that, for the same μ and different β, the tracking for unstable steady states appears to last longer for the higher value of β. And stronger β is needed to achieve the same tracking effect for smaller $|\mu|$.

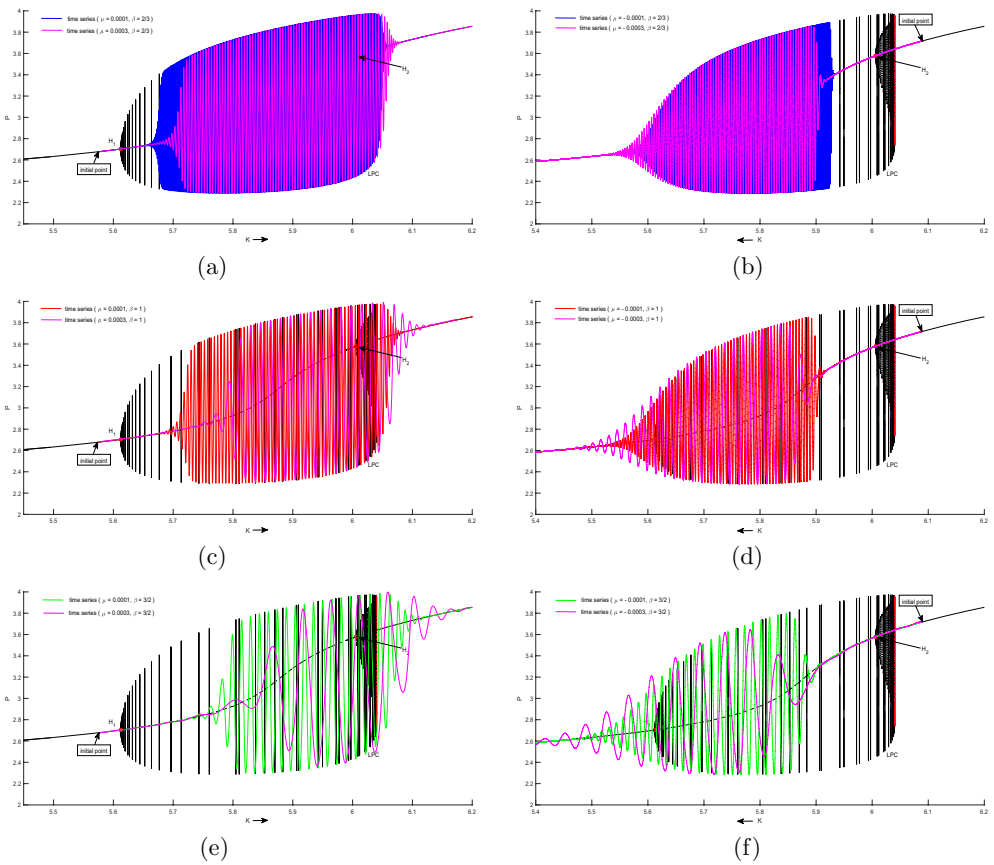

Figure 3.3. *Time series of system* (1.1) *for different* β *and* μ. *Initial population densities are near the stable steady state.* (a), (c), (e) $(N_0, P_0, K(0)) = (0.5394, 2.676, 5.574)$; (b), (d), (f) $(N_0, P_0, K(0)) = (1.65, 3.719, 6.09)$. *Other parameters are the same as those in Figure* 3.1.

The above analyses indicate that the regime shifts in a changing environment tend to occur at points that are not the bifurcation points of bifurcation diagrams, the direction of environmental changes can alter the shifting points, and the process is irreversible. Therefore, results here demonstrate the importance of μ, β, and the unstable states when describing the rate dependent transient dynamics in a changing environment.

Slow and fast regime shifts. For the same μ, β and initial conditions in Figure 3.3, the shift to the stable oscillation takes a relatively longer time than that to the stable steady state. The reason is that there is an unstable steady state that the solution of system (1.1) can and does follow before the shift to the stable oscillation. But when the shift to the stable steady state occurs, the solution of system (1.1) is far away from the boundary unstable states and is much more strongly attracted to the stable steady state.

In Figure 3.4, the initial population densities are close to the stable steady state. The solution of system (1.1) with the same fixed μ and β will take a longer time to the stable oscillation when the initial carrying capacity K_0 is farther away from the bifurcation point $\mathrm{H_i}$, and eventually synchronizes.

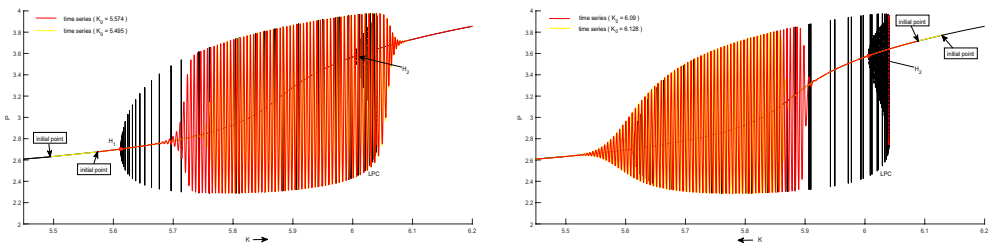

(a) (b)

Figure 3.4. *Time series of system* (1.1) *for different initial conditions.* (a) $\beta = 1$, $\mu = 0.0001$, $(N_0, P_0, K(0)) = (0.5394, 2.676, 5.574)$ *(red solid curve),* $(N_0, P_0, K(0)) = (0.5046, 2.63, 5.495)$ *(yellow solid curve);* (b) $\beta = 1$, $\mu = -0.0001$, $(N_0, P_0, K(0)) = (1.65, 3.719, 6.09)$ *(red solid curve),* $(N_0, P_0, K(0)) = (1.727, 3.77, 6.128)$ *(yellow solid curve). Other parameters are given in Figure* 3.1.

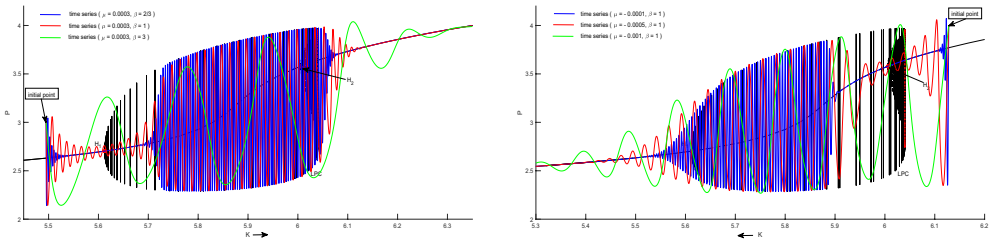

(a) (b)

Figure 3.5. *Time series of system* (1.1) *for different* β *and* μ*. Initial population densities are not close to the stable steady state.* (a) $(N_0, P_0, K(0)) = (0.5046, 3, 5.495)$*;* (b) $(N_0, P_0, K(0)) = (1.727, 4, 6.128)$*. Other parameters are given in Figure* 3.1.

Hence, the existence and location of unstable steady states in bifurcation diagrams and the initial conditions are crucial for predicting the dynamical behaviors and regime shifts of system (1.1) in a changing environment.

Different values of speed ($|\mu|$) or intensity (β) induce different transient dynamics. In Figure 3.5 the initial population densities are not close to the stable steady state. When the change of K is slow, i.e., $|\mu|$ or β is small, the solution (blue solid curves) first tracks the stable steady state for some time. When the change of K is fast, i.e., $|\mu|$ or β is large, there is no time for the solution to track the stable steady state; instead the solution (green solid curves) directly tracks the stable oscillation. When the change of K is intermediate (red solid curves), the time for the solution to approach the stable steady state is short enough so that the downturn along the stable steady state does not happen. Instead, the solution tracks the oscillation with a small amplitude before it switches to the stable big oscillation, which is a regime that does not occur in a constant environment.

Figure 3.6 shows that although the final state for all curves of system (1.1) is the same, the transient states of the solutions will be very different for the same β and different μ. There are at most five different transient dynamics with the change of μ. For example, the solution finally approaches the lower coexistence steady state but has five different transient dynamics in Figure 3.6(b) with the increase of $|\mu|$: (i) tracking first the higher stable coexistence steady state (the blue solid curve); (ii) tracking first the lower unstable small oscillation and then

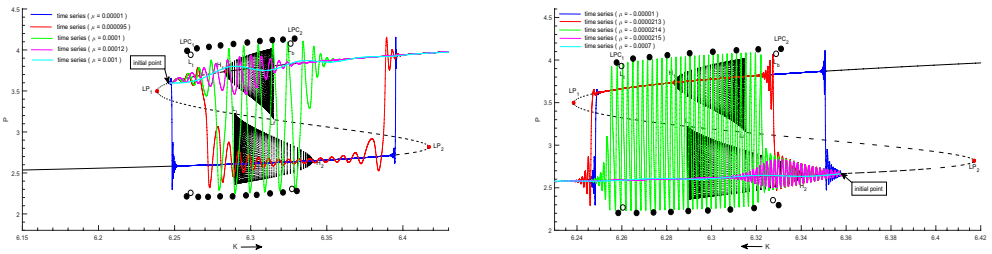

(a) (b)

Figure 3.6. *Time series of system* (1.1) *for* $\beta = 1$ *and different* μ. *Initial population densities are near one of the unstable steady states.* (a) $(N_0, P_0, K(0)) = (1.4, 3.597, 6.246)$; (b) $(N_0, P_0, K(0)) = (0.494, 2.666, 6.358)$. *Other parameters are the same as those in Figure* 3.2.

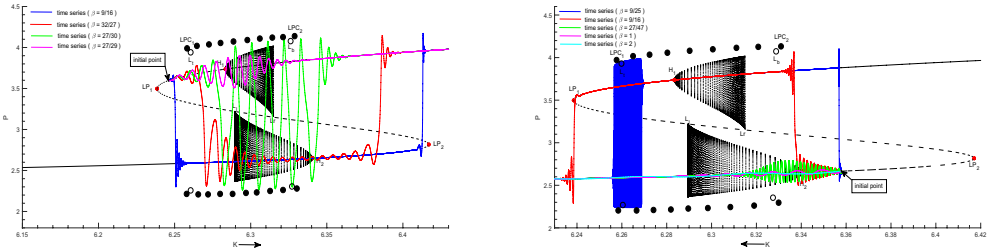

(a) (b)

Figure 3.7. *Time series of system* (1.1) *for different* β, *where initial population densities are near one of the unstable steady states.* (a) $\mu = 0.00015$, $(N_0, P_0, K(0)) = (1.4, 3.597, 6.246)$; (b) $\mu = -0.00015$, $(N_0, P_0, K(0)) = (0.494, 2.666, 6.358)$. *Other parameters are given in Figure* 3.2.

the higher stable coexistence steady state (the red solid curve); (iii) tracking first the lower unstable small oscillation and then the stable big oscillation (the green solid curve); (iv) tracking first the lower unstable small oscillation and then the lower stable coexistence steady state (the magenta solid curve); (v) tracking directly the lower coexistence steady state (the cyan solid curve). Figure 3.7 shows similar phenomena for the same μ but different β.

Hence, the results here again indicate the importance of the rate μ and intensity β of environmental change to induce different transient dynamics.

Tracking unstable oscillations. From Figures 3.6 and 3.7, we can see that the solutions of system (1.1) can track not only the unstable steady states but also the unstable oscillations, such as the red, green, and magenta curves in Figure 3.6(b). Figure 3.7 shows similar phenomena with fixed μ but different β.

Delay or avoid extirpation. When we initialize conditions near the stable coexistence steady state, and choose $\mu < 0$, then we can observe that the larger $|\mu|$ or β the farther the shift point is from the H_2 point (Figures 3.3(b), (d), (f)). While when we initialize conditions close to the unstable coexistence steady state, and choose $\mu < 0$ in Figures 3.8(a), (c), then we can observe that for small $|\mu|$ or β, the solutions (the blue solid curves) first follow the stable coexistence steady state and then approach the predator-only steady state after the LP point. For an intermediate $|\mu|$ or β, the solutions (the red solid curves) immediately follow the stable predator-only steady state. For large $|\mu|$ or β, there is no time for the solutions (the green

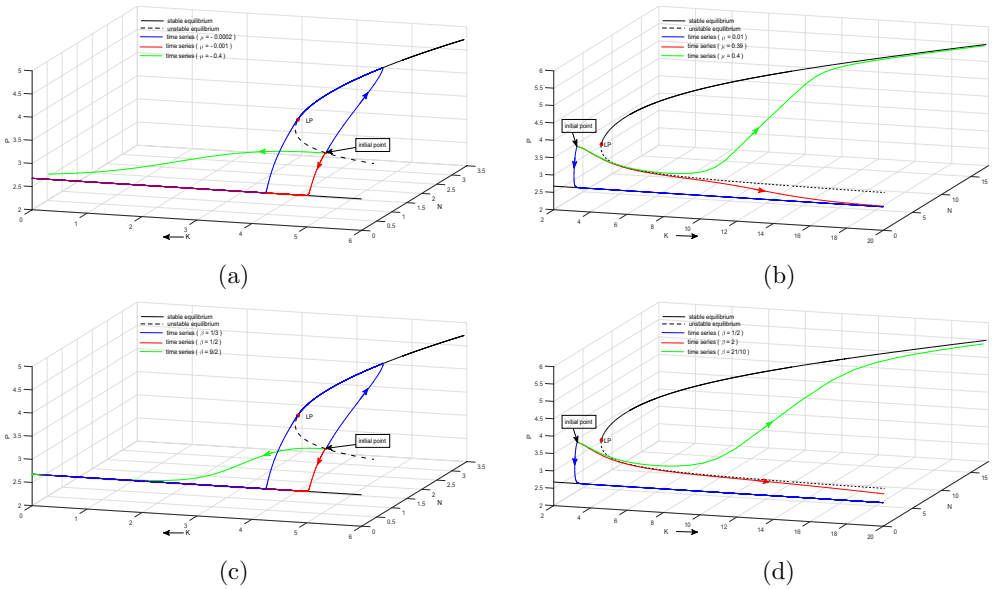

Figure 3.8. *One-parameter bifurcation diagrams (black color curves) in K-N-P space for system* (1.2). *Integral curves of system* (1.1) *for different* μ *and* β *are colored curves.* (a), (b) $\beta = 1$; (c) $\mu = -0.01$; (d) $\mu = 0.1$. *Initial conditions:* (a), (c) $(N_0, P_0, K(0)) = (0.5112, 3.397, 5.075)$; (b), (d) $(N_0, P_0, K(0)) = (0.9139, 3.767, 3)$. *LP denotes saddle-node bifurcation.* $A = 1$, $\gamma = \frac{1}{2}$, $\alpha = 1$, $R = \frac{5}{2}$, $M = \frac{6}{5}$, $C = \frac{605}{196}$, $Q = \frac{587}{1000}$.

solid curves) to approach the stable coexistence steady state or predator-only steady state. In fact, in the limiting case of very fast change of K, the population density would remain constant.

Letting $\mu > 0$ and initial population densities not be close to the steady state, and in Figures 3.8(b), (d), we can see that, for small $|\mu|$ or β, the solution (the blue solid curve) immediately follows the stable predator-only steady state that one would have predicted from the bifurcation diagram in a constant environment; thus the populations quickly tend to extinction. For an intermediate rate of change, the solution (the red solid curve) tracks first the unstable coexistence steady state and then switches to the predator-only steady state; thus the populations delay extinctions. When the change of K is fast, i.e., $|\mu|$ or β is large, the solution (the green solid curve) tracks first the unstable coexistence steady state and then switches quickly to the stable coexistence steady state; thus the populations avoid extirpation.

Hence, slow negative or fast positive environmental change can be beneficial to the population by avoiding or delaying extirpation.

4. Concluding remarks.

We studied the impact of nonlinear environmental change on the Rosenzweig–MacArthur model with generalist predator, where the predator can persist by switching to other food sources in the absence of the focal prey, and the prey's carrying capacity is a nonlinear function of time t.

In a constant environment $\mu = 0$, system (1.1) becomes system (1.2), which always has three boundary equilibria and at most three positive equilibria. By using some algebraic methods including resultant elimination, complete discrimination system for polynomials in

Yang [39], the realroot isolation algorithm, and Sturm's theorem to solve the semialgebraic varieties of normal form coefficients, we show that the highest codimension of a nilpotent focus is 4 and system (1.2) can exhibit nilpotent focus bifurcation of codimension 4, which includes a series of bifurcations with lower codimension [18, 20], such as *codimension* 1: saddle-node, Hopf, homoclinic, saddle-node of limit cycle, pitchfork bifurcations; *codimension* 2: degenerate Hopf, Bogdanov–Takens, degenerate homoclinic, saddle-node homoclinic, triple loop, double homoclinic, Hopf-Hopf, Hopf-saddle node, Hopf-homoclinic, symmetric nilpotent, cuspidal bifurcations; *codimension* 3: saddle-node bifurcation of limit cycle simultaneously with Bogdanov–Takens bifurcation, cuspidal loop bifurcation, limit cycle bifurcation of multiplicity four, Hopf bifurcation simultaneously with Bogdanov–Takens bifurcation, degenerate Hopf bifurcation simultaneously with saddle-node bifurcation, degenerate Bogdanov–Takens, a bottom homoclinic loop bifurcation of order three, nilpotent focus bifurcation. Our results indicate that codimension 4 nilpotent focus is the potential organizing center of the bifurcation set in system (1.2).

Comparing our results in Lemma 2.1 and Theorems 2.6, 2.7, and 2.8 about the Rosenzweig–Macarthur model (1.2) with generalist predator to the dynamics in the Rosenzweig–Macarthur model with specialist predator, we can see that generalist predation can cause richer bifurcations and dynamics, such as nilpotent focus bifurcation of codimension 4, multitype tristability (two positive equilibria and one big limit cycle; a positive equilibrium, one small limit cycle, and one big limit cycle; a positive equilibrium and two big limit cycles; two positive equilibria and one small limit cycle), multitype four stable states (two positive equilibria and two big limit cycles; two positive equilibria, one small limit cycle and one big limit cycle), and a figure-eight loop. Moreover, generalist predation can induce the persistence of predators for all positive initial densities and the extinction of the prey for some positive initial densities.

Compared with that in [10], we provided a more easily verifiable classification, in terms of the coefficients of the system with nilpotent linear part and general higher terms, to determine the types and codimension of nilpotent singularities in a general planar system. Our classification can be easily applied to other mathematical models with nilpotent singularities.

In a changing environment, i.e., $\mu \neq 0$ in system (1.1), we studied the effect of the rate μ and intensity β of nonlinear environmental change, and found multiple important characteristics about the asymptotic behaviors and transient dynamics for interacting species. Arumugam, Guichard, and Lutscher [3, 4] considered a linear environmental change (i.e., $\beta = 1$) in the carrying capacity, while here we consider a general environmental change (i.e., $\beta > 0$) including linear and nonlinear cases. Tracking unstable states was originally explored by Arumugam, Lutscher, and Guichard [4] in a single patch model, and extensively observed by Arumugam, Guichard, and Lutscher [3] in a two patch model. Arumugam, Guichard, and Lutscher [3] also investigated the rate induced extinction in a single patch. However, phenomena (b), (c), and (d) in section 3 were observed by Arumugam, Lutscher, and Guichard [4] or [3] only in a two patch model. Our results indicate that, for fixed environmental change rate μ, increasing or decreasing the intensity β of environmental change can achieve the same effects, i.e., phenomena (a)–(d) can be observed in our single patch model. Moreover, we found that slow negative or fast positive environmental change can delay or avoid population extirpation.

Appendix I. The coefficients in (2.5).

$$c_{30}=a_{30}+a_{20}b_{02},\quad c_{21}=\tfrac{1}{2}(a_{11}^2-4a_{02}a_{20}+2a_{21}+3a_{11}b_{02}),\quad c_{12}=-a_{02}a_{11}+a_{12}+2a_{02}b_{02},$$
$$c_{40}=\tfrac{1}{4}(2a_{11}(a_{30}-2a_{20}b_{02})-3a_{20}b_{02}^2+2a_{30}b_{02}+4a_{02}a_{20}^2-a_{11}^2a_{20}-4a_{20}a_{21}+4a_{40}),$$
$$c_{22}=\tfrac{1}{2}\Big[a_{02}\left(-3a_{11}b_{02}-2(a_{21}+b_{02}^2)+a_{11}^2\right)+3a_{12}b_{02}+4a_{20}a_{02}^2-a_{11}a_{12}-6a_{03}a_{20}+2a_{22}\Big],$$
$$\begin{aligned}c_{50}=\tfrac{1}{4}\Big[&a_{11}^2(5a_{20}b_{02}+a_{30})+a_{11}(7a_{20}b_{02}^2+2a_{30}b_{02}-4a_{02}a_{20}^2+4a_{40})+3a_{20}b_{02}^3+a_{30}b_{02}^2\\&-4a_{02}a_{20}^2b_{02}+4a_{40}b_{02}+a_{20}a_{11}^3+4a_{12}a_{20}^2-4a_{20}a_{31}+4a_{50}\Big],\end{aligned}$$
$$d_{20}=b_{20},\quad d_{11}=2a_{20}+b_{11},\quad d_{12}=a_{02}\,(4a_{20}+b_{11})+2b_{02}^2+b_{12},\quad d_{03}=b_{03}-2a_{02}b_{02},$$
$$d_{30}=-a_{20}b_{11}+a_{11}b_{20}+b_{30},\quad d_{21}=\tfrac{1}{2}(-8a_{20}b_{02}+a_{11}b_{11}+b_{02}b_{11}+4a_{02}b_{20}+2b_{21}),$$
$$\begin{aligned}d_{31}=&a_{11}(3a_{20}b_{02}+2a_{02}b_{20}+b_{21})+a_{20}b_{02}^2-a_{30}b_{02}-2a_{20}b_{12}-2a_{02}(a_{20}b_{11}+2a_{20}^2\\&+b_{02}b_{20}-b_{30})+a_{20}a_{11}^2+2a_{20}a_{21}+b_{02}b_{21}+b_{31},\end{aligned}$$
$$d_{13}=2a_{02}^2(2a_{20}+b_{11})+a_{02}b_{02}(a_{11}+2b_{02})-a_{12}b_{02}+2a_{03}a_{20}+2b_{02}b_{03}+b_{13},$$
$$\begin{aligned}d_{40}=\tfrac{1}{4}\Big[&12a_{20}^2b_{02}+a_{11}^2b_{20}-2a_{11}b_{02}b_{20}+b_{02}^2b_{20}+2a_{20}(4a_{30}-a_{11}b_{11}+b_{02}b_{11}-2b_{21})\\&+6a_{11}b_{30}+2b_{02}b_{30}+4b_{40}\Big],\end{aligned}$$
$$\begin{aligned}d_{41}=\tfrac{1}{4}\Big[&a_{11}^2(-15a_{20}b_{02}+2a_{02}b_{20}+b_{21})+2a_{11}(-8a_{20}b_{02}^2-a_{30}b_{02}-2a_{20}b_{12}\\&+a_{02}(-2a_{20}b_{11}+8a_{20}^2-6b_{02}b_{20}+6b_{30})+b_{21}b_{02}+3b_{31})-a_{20}b_{02}^3+2a_{30}b_{02}^2\\&+36a_{02}a_{20}^2b_{02}+4a_{20}a_{21}b_{02}-4a_{40}b_{02}+12a_{20}^2b_{03}+12a_{02}a_{20}b_{02}b_{11}-4a_{20}b_{02}b_{12}\\&+10a_{02}b_{02}^2b_{20}-8a_{02}a_{20}b_{21}-8a_{20}b_{22}-4a_{02}b_{02}b_{30}+8a_{02}b_{40}-4a_{20}a_{11}^3\\&-16a_{12}a_{20}^2+16a_{02}a_{20}a_{30}+8a_{20}a_{31}+b_{02}^2b_{21}+6b_{02}b_{31}+4b_{41}\Big].\end{aligned}$$

Appendix II. The proofs of Lemmas 2.3–2.5.

(A). The proof of Lemma 2.3. In general, we can use the method of normal form (see Chapter 2 of [11]) and the method of undetermined coefficients to get the normal forms. We just describe the methods as follows.

Assume the terms with order less than k ($k\geq 3$) of system (2.5) are already in normal form. We next simplify the kth terms, where the form of the kth terms is known but with undetermined coefficients. By the normal form theory (Chapter 2 of [11]), there exists a sequence of near identity transformations,

$$(x,y)=(X,Y)+(h_k^1(X,Y),h_k^2(X,Y)),$$

where $h_k^i(X,Y)$ ($i=1,2$) is a homogeneous polynomial of order k in (X,Y) with undetermined coefficients. Then differentiating the two sides of the above transformation with respect to t, substituting the old system and the above transformation into the left side, and equating the coefficients of the similar terms on the two sides, we can get the coefficients of the transformation and the new system. With $k=3,\ 4,\ 5$, we can transform system (2.5) into system (2.6), where j_{ij} can be expressed by c_{ij} and d_{ij}; we omit them for brevity.

(B). The proof of Lemma 2.4.

Step 1. Notice that $j_{20}=d_{20}\neq 0$; we let $x=X+\frac{j_{21}}{3j_{20}}XY+\frac{5j_{21}^2}{54j_{20}}X^4$, $y=Y+\frac{j_{21}}{3j_{20}}Y^2+\frac{j_{21}}{3}X^3+\frac{j_{21}j_{30}}{3j_{20}}X^4+\frac{10j_{21}^2}{27j_{20}}X^3Y$. Then the system (2.6) is changed into

(A.1)
$$\begin{aligned}\dot{X} &= Y + l_{50}X^5 + l_{41}X^4Y + o(|X,Y|^5),\\ \dot{Y} &= p_{20}X^2 + p_{30}X^3 + p_{40}X^4 + p_{31}X^3Y + p_{50}X^5 + p_{41}X^4Y + p_{32}X^3Y^2 + p_{23}X^2Y^3 + o(|X,Y|^5).\end{aligned}$$

Step 2. Let $X = x + \frac{4l_{41}+p_{32}}{20}x^5 + \frac{p_{23}}{12}x^4y$, $Y = y - l_{50}x^5 + \frac{p_{32}}{4}x^4y + \frac{p_{23}}{3}x^3y^2$. Then system (A.1) becomes

(A.2)
$$\begin{aligned}\dot{x} &= y + o(|x,y|^5),\\ \dot{y} &= r_{20}x^2 + r_{30}x^3 + r_{40}x^4 + r_{31}x^3y + r_{50}x^5 + r_{41}x^4y + o(|x,y|^5).\end{aligned}$$

Step 3. Notice that $r_{20} = d_{20} \neq 0$; let

$$\begin{aligned}x &= X - \tfrac{r_{30}}{4r_{20}}X^2 + \tfrac{15r_{30}^2-16r_{20}r_{40}}{80r_{20}^2}X^3 + \tfrac{-175r_{30}^3+336r_{20}r_{40}r_{30}-160r_{20}^2r_{50}}{960r_{20}^3}X^4,\\ y &= Y, \quad \tfrac{dt}{d\tau} = (1 - \tfrac{r_{30}}{2r_{20}}X + \tfrac{3(15r_{30}^2-16r_{20}r_{40})}{80r_{20}^2}X^2 + \tfrac{-175r_{30}^3+336r_{20}r_{40}r_{30}-160r_{20}^2r_{50}}{240r_{20}^3}X^3).\end{aligned}$$

Then system (A.2) becomes

(A.3)
$$\begin{aligned}\dot{X} &= Y + o(|X,Y|^5),\\ \dot{Y} &= s_{20}X^2 + s_{31}X^3Y + s_{41}X^4Y + o(|X,Y|^5).\end{aligned}$$

Step 4. Notice that $s_{20} = d_{20} \neq 0$; letting

$$X = \operatorname{sign}(s_{20})x, \quad Y = \operatorname{sign}(s_{20})\sqrt{\operatorname{sign}(s_{20})s_{20}}\,y, \quad \tfrac{d\tau}{dt} = \tfrac{1}{\sqrt{\operatorname{sign}(s_{20})s_{20}}},$$

we have

(A.4)
$$\begin{aligned}\dot{x} &= y + o(|x,y|^5),\\ \dot{y} &= x^2 + \bar{M}x^3y + \bar{N}x^4y + o(|x,y|^5),\end{aligned}$$

where

(A.5)
$$\bar{M} = \frac{M_1}{(\operatorname{sign}(d_{20})d_{20})^{\frac{3}{2}}}, \quad \bar{N} = \frac{N_1}{4(\operatorname{sign}(d_{20})d_{20})^{\frac{5}{2}}}$$

with

$$\begin{aligned}M_1 &= -c_{12}d_{20}^2 + 4c_{40}d_{20} - 3c_{30}d_{30} - 3d_{03}d_{20}^2 + d_{31}d_{20} - d_{21}d_{30},\\ N_1 &= -4c_{22}d_{20}^3 - 8c_{21}c_{30}d_{20}^2 + 20c_{50}d_{20}^2 - 2c_{30}d_{12}d_{20}^2 + c_{12}d_{30}d_{20}^2 - 20c_{40}d_{30}d_{20}\\ &\quad - 12c_{30}d_{40}d_{20} + 15c_{30}d_{30}^2 - 6d_{13}d_{20}^3 + 2d_{12}d_{21}d_{20}^2 + 3d_{03}d_{30}d_{20}^2 + 4d_{41}d_{20}^2\\ &\quad - 5d_{30}d_{31}d_{20} - 4d_{21}d_{40}d_{20} + 5d_{21}d_{30}^2,\end{aligned} \tag{A.6}$$

and c_{ij} and d_{ij}, expressed by a_{ij} and b_{ij}, are given in Appendix I.

Last we set $x = x$, $y = y + o(|x,y|^5)$ and then obtain the system (2.7). By Zhang et al. [41], Chow, Li, and Wang [11], Dumortier, Roussarie, and Sotomayor [13], and Li and Rousseau [21], we obtain the conclusions.

(C). The proof of Lemma 2.5.

Step 1. Notice that $j_{30} = d_{30} \neq 0$; we let

$$x = X - \tfrac{j_{40}}{5j_{30}}X^2, \quad y = Y, \quad \tfrac{dt}{d\tau} = 1 - \tfrac{2j_{40}}{5j_{30}}X.$$

Then system (2.6) becomes

$$\begin{aligned} \dot{X} &= Y + o(|X,Y|^4), \\ \dot{Y} &= q_{11}XY + q_{30}X^3 + q_{21}X^2Y + q_{31}X^3Y + o(|X,Y|^4) \end{aligned} \tag{A.7}$$

with

$$\begin{aligned} &q_{11} = d_{11}, \quad q_{30} = d_{30}, \quad q_{21} = \tfrac{3c_{30}(d_{11}^2+5d_{30})+5d_{21}d_{30}-3d_{11}d_{40}}{5d_{30}}, \\ &q_{31} = \tfrac{2c_{30}^2(d_{11}^3+30d_{30}d_{11})}{25d_{30}^2} - \tfrac{4c_{30}(d_{40}d_{11}^2-5d_{21}d_{30}d_{11}+15d_{30}d_{40})}{25d_{30}^2} + \tfrac{c_{21}d_{11}}{3} + 4c_{40} + \tfrac{2d_{11}d_{40}^2}{25d_{30}^2} + \tfrac{d_{11}d_{12}}{6} \\ &\quad + d_{31} - \tfrac{4d_{21}d_{40}}{5d_{30}}. \end{aligned} \tag{A.8}$$

Step 2. Notice that $q_{30} \neq 0$, $q_{21} \neq 0$; we let

$$X = \operatorname{sign}(q_{30}q_{21})\tfrac{\sqrt{\operatorname{sign}(q_{30})q_{30}}}{q_{21}}x, \quad Y = \tfrac{q_{30}\sqrt{\operatorname{sign}(q_{30})q_{30}}}{q_{21}^2}y, \quad \tfrac{d\tau}{dt} = \operatorname{sign}(q_{30}q_{21})\tfrac{q_{21}}{q_{30}},$$

and set $x = x$, $y = y + o(|x,y|^4)$; then obtain the system (2.8) from system (4.8), where

$$\begin{aligned} N_2 = {} & \tfrac{\operatorname{sign}(d_{30})\sqrt{\operatorname{sign}(d_{30})d_{30}}}{6(3c_{30}d_{11}^2+15c_{30}d_{30}-3d_{40}d_{11}+5d_{21}d_{30})^2}(12c_{30}^2d_{11}^3 - 24c_{30}d_{40}d_{11}^2 + 50c_{21}d_{30}^2d_{11} \\ & + 360c_{30}^2d_{30}d_{11} + 120c_{30}d_{21}d_{30}d_{11} + 600c_{40}d_{30}^2 - 360c_{30}d_{30}d_{40} + 25d_{12}d_{30}^2d_{11} \\ & + 12d_{40}^2d_{11} + 150d_{30}^2d_{31} - 120d_{21}d_{30}d_{40}). \end{aligned} \tag{A.9}$$

By Lemma 3.1 in [10], Dumortier et al. [15], Dumortier, Fiddelaers, and Li [12], Khibnik, Krauskopf, and Rousseau [20], and Dangelmayr and Guckenheimer [18], we get the results.

Appendix III. The proof of Theorem 2.6.

Step 1. When the conditions in (2.15) are satisfied and $(x_*, a, q) \in \Omega_1$, we make the following transformations successively,

$$\begin{aligned} &x = \hat{x} + x_*, \quad y = \hat{y} + y_*, \\ &\hat{x} = \frac{1}{1-a-2x_*}X + \frac{a+x_*}{x_*(1-a-2x_*)^2}Y, \quad \hat{y} = X, \end{aligned} \tag{A.10}$$

and following (2.5) and Appendix I, we have

$$\begin{aligned} d_{20} = {} & \frac{x_*^2(1-2a-3x_*-q(a+x_*)^3)}{(a+x^*)^3(1+aq(1-x_*)+qx_*(1-x_*))}, \\ d_{11} = {} & \frac{-a^2+a(1-3x_*)-x_*(1-2x_*+2x_*^2)+q(1-x_*)(a+x_*)^2(1-6x_*+6x_*^2-a(1-2x_*))}{(1-x_*)(a+x^*)^2(1-a-2x_*)(1+aq(1-x_*)+qx_*(1-x_*))}, \end{aligned}$$

where $d_{20} \neq 0$ since $q \neq q_1$ in Ω_1. Solving $d_{11} = 0$, we have $q = q_*$. Therefore, E_* is a cusp of codimension 2 if $q \neq q_*$ from Lemma 2.2.

Step 2. When $q = q_*$, we derive conditions for E_*, which is a cusp of codimension at least 3. It is easy to get

$$d_{20} = \frac{x_*(1-6x_*+4x_*^2-a)}{2(a+x^*)^2(1-x_*)},\ q_* - q_1 = \frac{(1-a-2x_*)^2(a-1+6x_*-4x_*^2)}{(1-x_*)(a+x_*)^3(1-6x_*+6x_*^2-a(1-2x_*))},$$
$$q_* - q_2 = \frac{x_*(1-a-2x_*)(-a^2-a(4x_*^2-x_*-1)-x_*(6x_*^2-6x_*+1))}{a(x_*-1)^2(a+x_*)^2(1-6x_*+6x_*^2-a(1-2x_*))},$$

and let

$$a_{1*} = \frac{1-6x_*+6x_*^2}{1-2x_*},\ a_{2*} = \frac{1+x_*-4x_*^2-(1-x_*)\sqrt{1+16x_*^2}}{2},$$
$$a_{3*} = \frac{1+x_*-4x_*^2+(1-x_*)\sqrt{1+16x_*^2}}{2},\ a_{4*} = \frac{1-3x_*-(1-x_*)\sqrt{1-8x_*}}{2},$$
$$a_{5*} = \frac{1-3x_*+(1-x_*)\sqrt{1-8x_*}}{2},\ a_{6*} = 1-6x_*+4x_*^2, \tag{A.11}$$

where $a = a_{1*}$ (resp., $a = a_{4*}$ and $a = a_{5*}$) come from the real root of the denominator (numerator) of q_*, $a = a_{2*}$ and $a = a_{3*}$ come from $q_* = q_2$, $a = a_{6*}$ comes from $q_* = q_1$.

Notice that $0 < a_{2*} < a_{1*} < 1-2x_* < a_{3*}$ if $\frac{1}{8} < x_* < \frac{3-\sqrt{3}}{6}$; $0 < a_{2*} < a_{4*} \le a_{6*} \le a_{5*} < a_{1*} < 1-2x_* < a_{3*}$ if $0 < x_* \le \frac{1}{8}$.

Then, we have the following conditions for x_* and a:

$$\Omega_2 = \Omega_{21} \cup \Omega_{22} \cup \Omega_{23},$$

where

$$\Omega_{21} = \left\{(x_*, a)\,|\,\frac{1}{8} < x_* < \frac{3-\sqrt{3}}{6},\ a_{2*} < a < a_{1*},\ a \neq a_{6*}\right\},$$
$$\Omega_{22} = \left\{(x_*, a)\,|\,0 < x_* \le \frac{1}{8},\ a_{2*} < a < a_{4*}\right\},$$
$$\Omega_{23} = \left\{(x_*, a)\,|\,0 < x_* \le \frac{1}{8},\ a_{5*} < a < a_{1*}\right\}. \tag{A.12}$$

Step 3. Next, we prove that E_* is a cusp of codimension at most 4. Following Lemma 2.4, (4.6), and (4.7), we have

$$M_1 = \frac{M_{1*}}{16x_*(1-a-2x^*)^5(a+x^*)^5(x^*-1)^4},\quad N_1 = \frac{N_{1*}}{64x_*(1-a-2x^*)^7(a+x^*)^8(x^*-1)^6},$$

where

$$\begin{aligned}M_{1*} =\ & a^6(2x_*-1)+2a^5(1-4x_*)(x_*^2-4x_*+2)+a^4(24x_*^5-132x_*^4+278x_*^3-207x_*^2+58x_*-6)\\ & -2a^3(16x_*^7-124x_*^6+372x_*^5-561x_*^4+403x_*^3-139x_*^2+25x_*-2)\\ & +a^2(-112x_*^8+632x_*^7-1456x_*^6+1748x_*^5-1082x_*^4+346x_*^3-72x_*^2+12x_*-1)\\ & -2ax_*(2x_*^2-4x_*+1)(32x_*^6-82x_*^5+66x_*^4+13x_*^3-37x_*^2+12x_*-1)\\ & -x_*^2(112x_*^8-592x_*^7+1304x_*^6-1552x_*^5+1080x_*^4-452x_*^3+114x_*^2-16x_*+1),\end{aligned}$$

$$\begin{aligned}N_{1*} =& a^9(-8x_*^2+14x_*-5)+a^8(64x_*^4-304x_*^3+428x_*^2-209x_*+30)+a^7(-224x_*^6+1728x_*^5\\ &-4792x_*^4+5896x_*^3-3319x_*^2+822x_*-75)+a^6(512x_*^8-4704x_*^7+18912x_*^6-39512x_*^5\\ &+44560x_*^4-27133x_*^3+8814x_*^2-1465x_*+100)+a^5(-512x_*^{10}+6560x_*^9-34016x_*^8\\ &+99440x_*^7-174996x_*^6+186130x_*^5-118776x_*^4+45398x_*^3-10357x_*^2+1330x_*-75)\\ &+a^4(-2944x_*^{11}+26176x_*^{10}-104000x_*^9+248032x_*^8-382204x_*^7+381932x_*^6-245366x_*^5\\ &+101980x_*^4-28067x_*^3+5136x_*^2-579x_*+30)+a^3(-6720x_*^{12}+48192x_*^{11}-151056x_*^{10}\\ &+278384x_*^9-331728x_*^8+256368x_*^7-121960x_*^6+33076x_*^5-5240x_*^4+1084x_*^3-385x_*^2\\ &+74x_*-5)+a^2(-9664x_*^{13}+64256x_*^{12}-180560x_*^{11}+277280x_*^{10}-239232x_*^9+83104x_*^8\\ &+50488x_*^7-78920x_*^6+45628x_*^5-14920x_*^4+2861x_*^3-298x_*^2+13x_*)+a(-9664x_*^{14}\\ &+71840x_*^{13}-239808x_*^{12}+479200x_*^{11}-641744x_*^{10}+607472x_*^9-415728x_*^8+206144x_*^7\\ &-72868x_*^6+17722x_*^5-2808x_*^4+262x_*^3-11x_*^2)-2240x_*^{15}+15680x_*^{14}-47904x_*^{13}\\ &+83648x_*^{12}-90832x_*^{11}+60864x_*^{10}-20928x_*^9-1632x_*^8+5380x_*^7-2564x_*^6+594x_*^5\\ &-68x_*^4+3x_*^3,\end{aligned}$$

and the signs of M_1 and N_1 are decided by M_{1*} and N_{1*}, respectively.

Note that the leading coefficient of the polynomial M_{1*} with respect to x_* is $\mathrm{lcoeff}(M_{1*}, x_*) = -112 \neq 0$. Furthermore, using the "resultant(M_{1*}, N_{1*}, x_*)" command in MAPLE, we have

$$\begin{aligned}\mathrm{res}(M_{1*}, N_{1*}, x_*) =& 135399691796838467567091712(a-1)^{27}a^{10}(a+1)^{59}(4a+1)^6(64a+71)^2\\ &(4096a^5+7872a^4+6528a^3+2288a^2+400a+17)\neq 0,\end{aligned}$$

since $0<a<1$ from conditions in Ω_2, where $\mathrm{res}(f,g,x)$ denotes the Sylvester resultant of f and g with respect to x. Then from Gelfand, Kapranov, and Zelevinsky [17], M_{1*} and N_{1*} have no common roots, which implies that $N_{1*}\neq 0$ if $M_{1*}=0$. Then, according to Lemma 2.4, E_* is a cusp of codimension at most 4.

Step 4. Letting

$$D_0 = \Big\{(x_*,\, a)\,|\,0<x_*<\frac{3-\sqrt{3}}{6},\ 0<a<a_{1*}\Big\}\supseteq\Omega_2,$$

we next use four steps to prove that $M_{1*}<0$ when $(x_*,\, a)\in D_0$.

Step 4.1. First, by applying Sturm's theorem, we have

$$\begin{aligned}&M_{1*}|_{a=0} = x_*^2\left(-112x_*^8+592x_*^7-1304x_*^6+1552x_*^5-1080x_*^4+452x_*^3-114x_*^2+16x_*-1\right)<0,\\ &M_{1*}|_{a=a_{1*}} = -\frac{128(1-x_*)x_*^5(1-4x_*)^2}{(1-2x_*)^4}<0\end{aligned}$$

with $0<x_*<\frac{3-\sqrt{3}}{6}$. Thus, Lemma 3.1 of [39] indicates that the number of roots for M_{1*} in the interval $(0,\, a_{1*})$ with $0<x_*<\frac{3-\sqrt{3}}{6}$ is equal to that of positive roots for

$$\begin{aligned}\Phi =&(1-2x_*)^5(1+a)^6M_{1*}\Big(\frac{a_{1*}}{1+a}\Big)\\ =&\Phi_6a^6+\Phi_5a^5+\Phi_4a^4+\Phi_3a^3+\Phi_2a^2+\Phi_1a+\Phi_0,\end{aligned}$$

where

$$\Phi_6 = x_*^2(1-2x_*)^5(-112x_*^8+592x_*^7-1304x_*^6+1552x_*^5-1080x_*^4+452x_*^3-114x_*^2+16x_*-1),$$
$$\Phi_5 = -2(1-x_*)x_*(1-2x_*)^4(288x_*^9-1464x_*^8+3368x_*^7-4692x_*^6+4392x_*^5-2710x_*^4+1022x_*^3 - 219x_*^2+24x_*-1),$$
$$\Phi_4 = -(1-x_*)^2(1-2x_*)^3(3072x_*^{10}-20352x_*^9+58240x_*^8-91888x_*^7+85176x_*^6-47808x_*^5 + 16580x_*^4-3548x_*^3+454x_*^2-32x_*+1),$$
$$\Phi_3 = -2(1-x_*)^3x_*(1-2x_*)^2(6272x_*^9-35360x_*^8+79200x_*^7-90152x_*^6+58120x_*^5-22540x_*^4 + 5320x_*^3-730x_*^2+50x_*-1),$$
$$\Phi_2 = -4(1-x_*)^4x_*^2(1-2x_*)(5184x_*^8-19968x_*^7+28448x_*^6-21024x_*^5+9660x_*^4-3024x_*^3 + 644x_*^2-84x_*+5),$$
$$\Phi_1 = 32(1-x_*)^5x_*^3(1-4x_*)(48x_*^6-122x_*^4+120x_*^3-51x_*^2+11x_*-1),$$
$$\Phi_0 = -128(1-x_*)^7x_*^5(1-2x_*)(1-4x_*)^2.$$

Thus, we only need to prove that $\Phi<0$ for $(a,x_*)\in(0,\infty)\times(0,\frac{3-\sqrt{3}}{6})$.

Step 4.2. Second, by applying Sturm's theorem, we have $\Phi_6<0$ and $\Phi_0<0$ for $0<x_*<\frac{3-\sqrt{3}}{6}$. And, by direct computation, we have

$$\Phi|_{x_*=0} = -a^4 \le 0, \quad \Phi|_{x_*=\frac{3-\sqrt{3}}{6}} = -\frac{2(-3+2\sqrt{3})(a+1)^6}{6561} < 0, \quad \Phi|_{a=0} = \Phi_0 \le 0,$$

where $\Phi|_{a=0}=0$ (resp., $\Phi|_{x_*=0}$) if and only if $x_*=0$ (resp., $a=0$). The leading coefficient of the polynomial Φ with respect to a is $\mathrm{lcoeff}(\Phi,a)=\Phi_6<0$ if $x_*>0$, or $\mathrm{lcoef}(\Phi,a)=\Phi_4|_{x_*=0}=-1<0$ if $x_*=0$. Thus, there exists a sufficiently large $N(x_*)$ such that $\Phi<0$ if $a\ge N(x_*)$ for any fixed $0\le x_*\le\frac{3-\sqrt{3}}{6}$. Letting $N_{x*}=\max_{0\le x_*\le\frac{3-\sqrt{3}}{6}}\{N(x_*)\}$, then $\Phi<0$ if $a\ge N_{x*}$ for any $0\le x_*\le\frac{3-\sqrt{3}}{6}$. Therefore, $\Phi\le 0$ at the boundary of the rectangular area

$$D_1 = \left\{(a,x_*)|0\le a\le N_{x*},\ 0\le x_*\le\frac{3-\sqrt{3}}{6}\right\},$$

and the equal sign is only taken at the point $(0,0)$. Thus, we just need to prove that $\Phi<0$ at the interior of the domain D_1.

Step 4.3. Third, we look for a possible domain where stationary points of Φ exist. By calculating the first-order partial derivatives of Φ with respect to a and x_*, respectively, we can get the expressions of $\frac{\partial\Phi}{\partial a}$ and $\frac{\partial\Phi}{\partial x_*}$, which are all 20-order polynomials of a and x_*; we omit them for brevity.

Then, eliminating the variable a (resp., x_*) by computing the resultant $\tilde{R}_1(x_*)$ (resp., $\tilde{R}_2(a)$) between $\frac{\partial\Phi}{\partial a}$ and $\frac{\partial\Phi}{\partial x_*}$, we obtain that

$$\tilde{R}_1(x_*) = 134217728x_*^{13}(1-4x_*)(1-2x_*)^{20}(1-x_*)^{25}(6x_*^2-6x_*+1)^{25}\tilde{R}_{11}(x_*),$$

$$\tilde{R}_2(a) = 1246151246048358630847319119012823 04a^{35}(a+1)^{56}\tilde{R}_{21}(a),$$

where $\tilde{R}_{11}(x_*)$ and $\tilde{R}_{21}(a)$ are 45-order polynomials of x_* and a, respectively; we omit them.

Notice that the signs of $\tilde{R}_1(x_*)$ and $\tilde{R}_2(a)$ are the same as $\tilde{R}_{11}(x_*)$ and $\tilde{R}_{21}(a)$, respectively. Through isolating the real roots of $\tilde{R}_{21}(a)$ by using the function "realroot" wirh accuracy $\frac{1}{1000}$ in MAPLE, we can prove that the root is in the closed subinterval

$$I_{11} = \Big[\frac{1975659}{8388608}, \frac{987831}{4194304}\Big] \triangleq \Big[\underline{I}_{11}, \overline{I}_{11}\Big]$$

contained in $(0, N_{x*})$.

Similarly, the root of $\tilde{R}_{11}(x_*)$ is in the closed subinterval

$$I_{21} = \Big[\frac{1491421}{16777216}, \frac{46607}{524288}\Big] \triangleq \Big[\underline{I}_{21}, \overline{I}_{21}\Big], \quad I_{22} = \Big[\frac{50189}{262144}, \frac{200759}{1048576}\Big] \triangleq \Big[\underline{I}_{22}, \overline{I}_{22}\Big]$$

contained in $(0, \frac{3-\sqrt{3}}{6})$.

Therefore, if the polynomials $\tilde{R}_{11}(x_*)$ and $\tilde{R}_{21}(a)$ have one common root $(a, x_*) \in D_1$, the point must be in the following two domains:

$$D_2 = \Big\{(a, x_*) \,|\, \underline{I}_{11} \le a \le \overline{I}_{11},\ \underline{I}_{21} \le x_* \le \overline{I}_{21}\Big\}$$

and

$$D_3 = \Big\{(a, x_*) \,|\, \underline{I}_{11} \le a \le \overline{I}_{11},\ \underline{I}_{22} \le x_* \le \overline{I}_{22}\Big\}.$$

Hence, the stationary points of polynomial Φ can only be achieved at the interior of D_2 and D_3; then extremal value of polynomial Φ can only be achieved at the boundary of D_1 and the interior of D_2 and D_3.

Step 4.4. At last, we prove that $\Phi < 0$ for all $(a, x_*) \in D_2 \cup D_3$. By direct computation, we obtain that the values of the function Φ at the four vertices of the rectangular domain D_2 are negative. By applying Sturm's theorem, we have that on one pair of opposite sides of D_2,

$$\Phi\Big(a = \underline{I}_{11}, x_*\Big) < 0, \quad \Phi\Big(a = \overline{I}_{11}, x_*\Big) < 0$$

for $\underline{I}_{21} \le x_* \le \overline{I}_{21}$.

With the same techniques, we can assert that on the other pair of opposite sides of D_1,

$$\Phi\Big(a, x_* = \underline{I}_{21}\Big) < 0, \quad \Phi\Big(a, x_* = \overline{I}_{21}\Big) < 0$$

for $\underline{I}_{11} \le a \le \overline{I}_{11}$. Hence the above arguments imply that $\Phi < 0$ on the boundary of the domain D_2. Thus, Lemma 3.1 of [39] indicates that the number of the roots for Φ in the domain D_2 is equal to that of roots in $(0, \infty) \times (0, \infty)$ for

$$\Phi^* = (1 + x_*)^{15} \Phi_*\Big(a, \frac{\overline{I}_{21} + \underline{I}_{21} x_*}{1 + x_*}\Big),$$

where

$$\Phi_*(a, x_*) = (1 + a)^6 \Phi\Big(\frac{\overline{I}_{11} + \underline{I}_{11} a}{1 + a}, x_*\Big).$$

From the expression of Φ^*, it is easy to see that $\Phi^* < 0$ in $(0,\infty)\times(0,\infty)$, which implies $\Phi < 0$ on the domain D_2. Similarly, we can assert that $\Phi < 0$ for all $(a, x_*) \in D_3$.

Summarizing the above results, based on the eliminating theory by resultant and the algorithm of real root isolation, it follows that $\Phi \le 0$ on domain D_1, and $\Phi = 0$ if and only if $(a, x_*) = (0,0)$. Thus, $\Phi < 0$ on the interior of the domain D_1. Then $M_{1*} < 0$ when $(x_*, a) \in D_0$, which implies $M_{1*} < 0$ when $(x_*, a) \in \Omega_2$, i.e., E_* is a cusp of codimension 3 by Lemma 2.4.

Appendix IV. The proof of Theorem 2.7.

Step 1. From (2.13), we have $\mathrm{Det}(J(E^*)) = 0$. When $b \neq b^*$ by Theorem 7.1 in chapter 2 of [41], E^* is an unstable degenerate node if $0 < b < b^*$ and a stable degenerate node if $b > b^*$.

Step 2. When $b = b^*$, we make the following transformations successively:

$$\begin{aligned} &x = \hat{x} + x^*, \quad y = \hat{y} + y^*, \\ &\hat{x} = \frac{1}{1-a-2x^*}X + \frac{a+x^*}{x^*(1-a-2x^*)^2}Y, \quad \hat{y} = X. \end{aligned} \tag{A.13}$$

Then system (2.1) becomes

$$\begin{aligned} \dot{X} &= Y + \sum_{2\le i+j\le 4} a_{ij}X^iY^j + o(|X,Y|^4), \\ \dot{Y} &= \sum_{2\le i+j\le 4} b_{ij}X^iY^j + o(|X,Y|^4); \end{aligned} \tag{A.14}$$

we omit expressions of a_{ij}, b_{ij} for brevity.

Then following (2.5) and Appendix I, system (A.15) becomes

$$\begin{aligned} \frac{dX}{dt} &= Y + \sum_{3\le i+j\le 4} c_{ij}X^iY^j + o(|X,Y|^4), \\ \frac{dY}{dt} &= d_{11}XY + \sum_{3\le i+j\le 5} d_{ij}X^iY^j + o(|X,Y|^4), \end{aligned} \tag{A.15}$$

where

$$\begin{aligned} c_{30} &= \frac{a - 2ax^* - x^{*2}}{(1-a-2x^*)^2(a+x^*)^2(x^*-1)}, \quad d_{11} = \frac{1-a-6x^*+4x^{*2}}{(1-a-2x^*)(a+x^*)(1-x^*)}, \\ d_{30} &= -\frac{x^{*2}}{(1-a-2x^*)^2(a+x^*)^2}, \\ d_{21} &= \frac{1}{2(x^*-1)^2x^*(a+x^*)^2(a+2x^*-1)^3}\Big(a^3(2x^*-1) + a^2(-4x^{*3}+12x^{*2}-7x^*+2) \\ &\quad - a(x^{*3}-2x^{*2}-3x^*+1) + x^*(10x^{*4}-32x^{*3}+35x^{*2}-14x^*+2)\Big), \\ d_{40} &= \frac{1}{2(x^*-1)^2(a+x^*)^3(a+2x^*-1)^4}\Big(a^3(4x^*-2) + a^2(-10x^{*3}+33x^{*2}-21x^*+4) \\ &\quad + a(-30x^{*4}+79x^{*3}-58x^{*2}+17x^*-2) + x^{*2}(-17x^{*3}+39x^{*2}-24x^*+4)\Big), \end{aligned}$$

and we omit other expressions of c_{ij}, d_{ij}. It is easy to see that $d_{30} < 0$ since conditions in (2.19) are satisfied.

By direct computation, we have

$$d_{11}^2+8d_{30}=\frac{S_1}{(x^*-1)^2(a+x^*)^2(a+2x^*-1)^2},$$
$$3c_{30}(d_{11}^2+5d_{30})+5d_{21}d_{30}-3d_{11}d_{40}=\frac{x^*S_2}{(x^*-1)^2(a+x^*)^3(1-a-2x^*)^5},$$

where

$$S_1=a^2-8ax^{*2}+12ax^*-2a+8x^{*4}-32x^{*3}+36x^{*2}-12x^*+1, \tag{A.16}$$

$$S_2=2a^2(1-2x^*)-4a(x^{*3}+2x^{*2}-3x^*+1)-11x^{*4}+10x^{*3}+5x^{*2}-8x^*+2. \tag{A.17}$$

Notice that the signs of $d_{11}^2+8d_{30}$ and $3c_{30}(d_{11}^2+5d_{30})+5d_{21}d_{30}-3d_{11}d_{40}$ are the same as S_1 and S_2, respectively.

From $S_2|_{a=a^{2*}}>0$ and $a^{2*}-\frac{x^{*3}+2x^{*2}-3x^*+1}{1-2x^*}=-\frac{(1-x_*)(1-2x_*^2)}{2(1-2x^*)}<0$, we have $S_2>0$, i.e., $3c_{30}(d_{11}^2+5d_{30})+5d_{21}d_{30}-3d_{11}d_{40}>0$ as conditions in (2.19) are satisfied.

Step 3. Next, we analyze the sign of d_{11} and S_1 to determine the types of E^*. The discriminant of S_1 with respect to a is $32x^{*2}(1-x^*)^2>0$. Solving $d_{11}=0$ (resp., $S_1=0$), we have $a=a_1^*$(resp., $a=a_2^*$ and $a=a_1^*+2\sqrt{2}(1-x^*)x^*\triangleq\overline{a}_2^*$), respectively, where a_1^* and a_2^* are given in (2.21). And direct computation gives

$$a_1^*-a^{1*}=\frac{1}{2}(1-x^*)(1-8x^*+\sqrt{1-4x^*}),\quad a_1^*-a^{2*}=\frac{1}{2}(1-x^*)(1-8x^*),$$

$$a_2^*-a^{1*}=\frac{1}{2}(1-x^*)(1-8x^*-4\sqrt{2}x^*+\sqrt{1-4x^*}),\quad a_2^*-a^{2*}=\frac{1}{2}(1-x^*)(1-8x^*-4\sqrt{2}x^*),$$

$$\overline{a}_2^*-a^{2*}=\frac{1}{2}(1-x^*)(1-4(2-\sqrt{2})x^*).$$

Notice that $\overline{a}_2^*>a^{2*}$ since $0<x^*<\frac{1}{4}$. And, we obtain $a_1^*\le a^{1*}$(resp., $a_1^*\ge a^{2*}$) if and only if $x^*\ge\frac{3}{16}$ (resp., $x^*\le\frac{1}{8}$); $a_2^*\le a^{1*}$(resp., $a_2^*\ge a^{2*}$) if and only if $x^*\ge\frac{1}{8}$ (resp., $x^*\le\frac{2-\sqrt{2}}{8}$). Thus, we have (i) $a_2^*<a_1^*\le a^{1*}$ if $\frac{3}{16}\le x_*<\frac{1}{4}$; (ii) $a_2^*<a^{1*}<a_1^*<a^{2*}$ if $\frac{1}{8}<x_*<\frac{3}{16}$; (iii) $a_2^*=a^{1*}<a^{2*}=a_1^*$ if $x_*=\frac{1}{8}$; (iv) $a^{1*}<a_2^*<a^{2*}<a_1^*$ if $\frac{2-\sqrt{2}}{8}<x_*<\frac{1}{8}$; (v) $a^{2*}\le a_2^*<a_1^*$ if $0<x_*\le\frac{2-\sqrt{2}}{8}$.

Combining conditions in (2.19) and analyzing the sign of d_{11}, S_1, we have the results in Table 2 by Lemma 2.5. Therefore, we have completed the proof.

Appendix V. The proof of Theorem 2.8.

Consider the following unfolding system:

$$\begin{aligned}\frac{dx}{dt}&=x(1-x-\frac{y}{a_1^*+\lambda_4+x}),\\ \frac{dy}{dt}&=y\Big[\frac{(b^*+\lambda_3)x}{a_1^*+\lambda_4+x}+\frac{c^*+\lambda_1+m^*+\lambda_2}{1+q^*y}-(m^*+\lambda_2)\Big],\end{aligned} \tag{A.18}$$

where $\lambda=(\lambda_1,\lambda_2,\lambda_3,\lambda_4)\triangleq(c-c^*,m-m^*,b-b^*,a-a_1^*)$ is a parameter vector in a small neighborhood of $(0,0,0,0)$.

Next we want to transform the unfolding system (2.22) into the versal unfolding of codimension 4 nilpotent focus by a series of near-identity transformations.

First, we make the following transformations successively:

$$\text{(I)}\ x=\hat{x}+x^*,\quad y=\hat{y}+y^*,$$
$$\text{(II)}\ \hat{x}=\frac{1}{1-a-2x^*}X+\frac{a+x^*}{x^*(1-a-2x^*)^2}Y,\quad \hat{y}=X.$$

Then system (2.22) becomes

$$\begin{aligned}\frac{dX}{dt}&=\sum_{0\le i+j\le 5}a_{ij}(\lambda)X^iY^j+o(|X,Y|^5),\\ \frac{dY}{dt}&=\sum_{0\le i+j\le 5}b_{ij}(\lambda)X^iY^j+o(|X,Y|^5),\end{aligned}\tag{A.19}$$

where $a_{ij}(\lambda)$ and $b_{ij}(\lambda)$ are smooth functions whose long expressions are omitted here for the sake of brevity.

Second, letting

$$\text{(III)}\ X=x+\frac{a_{11}(\lambda)+b_{02}(\lambda)}{2}x^2,\quad Y=y-a_{20}(\lambda)x^2+b_{02}(\lambda)xy-a_{02}(\lambda)y^2,$$

system (A.19) becomes

$$\begin{aligned}\frac{dx}{dt}&=\sum_{0\le i+j\le 3}c_{ij}(\lambda)x^iy^j+o(|x,y|^3),\\ \frac{dy}{dt}&=\sum_{0\le i+j\le 3}d_{ij}(\lambda)x^iy^j+o(|x,y|^3),\end{aligned}\tag{A.20}$$

where $c_{ij}(\lambda)$ and $d_{ij}(\lambda)$ are smooth functions whose long expressions are omitted here.

Third, we make

$$\textbf{(IV)}\ \begin{cases}x=X+\frac{2c_{21}(\lambda)+d_{12}(\lambda)}{6}X^3+\frac{c_{12}(\lambda)+d_{03}(\lambda)}{2}X^2Y+c_{03}(\lambda)XY^2,\\ y=Y-c_{30}(\lambda)X^3+\frac{d_{12}(\lambda)}{2}X^2Y+d_{03}(\lambda)XY^2.\end{cases}$$

System (A.20) then becomes

$$\begin{aligned}\frac{dX}{dt}&=Y+\sum_{0\le i+j\le 3}e_{ij}(\lambda)X^iY^j+o(|X,Y|^3),\\ \frac{dY}{dt}&=\sum_{0\le i+j\le 3}f_{ij}(\lambda)X^iY^j+o(|X,Y|^3),\end{aligned}\tag{A.21}$$

where $e_{ij}(\lambda)$ and $f_{ij}(\lambda)$ are smooth functions whose long expressions are omitted here.

Fourth, we make the smooth coordinate transformation

$$\text{(V)}\ x_1=X,\quad y_1=\frac{dX}{dt};$$

then system (A.21) becomes

$$\begin{aligned} \frac{dx_1}{dt} &= y_1, \\ \frac{dy_1}{dt} &= \sum_{0\le i+j\le 3} \bar{f}_{ij}(\lambda) x_1^i y_1^j + o(|x_1, y_1|^3), \end{aligned} \tag{A.22}$$

where $\bar{f}_{ij}(\lambda)$ can be expressed by $\lambda_1, \lambda_2, \lambda_3, \lambda_4$, and x^*; we omit their expressions.

Fifth, notice that $\bar{f}_{ij}(0) = 0$ $(0 \le i + j \le 2)$, $\bar{f}_{12}(0) = \bar{f}_{03}(0) = 0$, and

$$\bar{f}_{30}(0) = d_{30} = \frac{-1}{16(1-4x^*)^2(1-x^*)^4} < 0, \quad \bar{f}_{21}(0) = 3c_{30} + d_{21} = -\frac{9-16x^*}{64(1-x^*)^4 x^{*2}(1-4x^*)} < 0$$

since $\frac{1}{8} < x^* < \frac{3}{16}$. We continue to make the following smooth coordinate transformations successively:

$$\begin{aligned} &\text{(VI)} \quad x_1 = x_2 - \frac{\bar{f}_{20}(\lambda)}{3\bar{f}_{30}(\lambda)}, \quad y_1 = y_2; \\ &\text{(VII)} \quad x_2 = \frac{\sqrt{-\bar{f}_{30}(\lambda)}}{\bar{f}_{21}(\lambda)} x, \quad y_2 = \frac{\bar{f}_{30}\sqrt{-\bar{f}_{30}(\lambda)}}{\bar{f}_{21}^2(\lambda)} y, \quad \frac{dt}{d\tau} = \frac{\bar{f}_{21}(\lambda)}{\bar{f}_{30}(\lambda)}. \end{aligned} \tag{A.23}$$

Then system (A.22) becomes as system (2.23) (still denoting τ by t), where $\mu_i(\lambda)(i = 1, 2, 3, 4)$ can be expressed by $\lambda_1, \lambda_2, \lambda_3, \lambda_4$, and x^*; we omit their detailed expressions.

Since

$$\begin{aligned} &\left| \frac{\partial(\mu_1(\lambda), \mu_2(\lambda), \mu_3(\lambda), \mu_4(\lambda))}{\partial(\lambda_1, \lambda_2, \lambda_3, \lambda_4)} \right|_{\lambda=0} \\ &= \frac{(9-16x^*)^6(1-4x^*)^5(1-6x^*+4x^{*2})(1-8x^*)(3-46x^*+64x^{*2})}{6291456(1-x^*)^2 x^{*15}} > 0 \end{aligned} \tag{A.24}$$

for $\frac{1}{8} < x^* < \frac{3}{16}$, the parameter transformation $(\lambda_1, \lambda_2, \lambda_3, \lambda_4) \to (\mu_1, \mu_2, \mu_3, \mu_4)$ is a homeomorphism in a small neighborhood of the origin, and μ_1, μ_2, μ_3, and μ_4 are independent parameters. By the results in [18, 20], we know that system (2.23) is a 4-parameter family versal unfolding of codimension 4 nilpotent focus. Hence, system (2.22) can undergo a nilpotent focus bifurcation of codimension 4 around E^*.

REFERENCES

[1] C. Aldebert, B. W. Kooi, D. Nerini, M. Gauduchon, and J.-C. Poggiale, *Three-dimensional bifurcation analysis of a predator-prey model with uncertain formulation*, SIAM J. Appl. Math., 79 (2019), pp. 377–395.

[2] A. Arsie, C. Kottegoda, and C. Shan, *A predator-prey system with generalized Holling type IV functional response and Allee effects in prey*, J. Differential Equations, 309 (2022), pp. 704–740.

[3] R. Arumugam, F. Guichard, and F. Lutscher, *Persistence and extinction dynamics driven by the rate of environmental change in a predator-prey metacommunity*, Theor. Ecol., 13 (2020), pp. 629–643.

[4] R. Arumugam, F. Lutscher, and F. Guichard, *Tracking unstable states: Ecosystem dynamics in a changing world*, Oikos, 130 (2021), pp. 525–540.

[5] S. M. Baer, B. W. Kooi, Yu A. Kuznetsov, and H. R. Thieme, *Multiparametric bifurcation analysis of a basic two-stage population model*, SIAM J. Appl. Math., 66 (2006), pp. 1339–1365.

[6] R. I. Bogdanov, *Bifurcations of the limit cycle of a family of plane vector fields*, Trudy Sem. Petrovsk., 2 (1976), pp. 23–35 (in Russian); Sel. Math. Sov., 1 (1981), pp. 373–387 (in English).
[7] R. I. Bogdanov, *Versal deformations of a singular point of a vector field on the plane in the case of zero eigenvalues*, Trudy Sem. Petrovsk., 2 (1976), pp. 37–65 (in Russian); Sel. Math. Sov., 1 (1981), pp. 389–421 (in English).
[8] H. W. Broer, V. Naudot, R. Roussarie, and K. Saleh, *Dynamics of a predator-prey model with non-monotonic response function*, Discrete Contin. Dyn. Syst. Ser. A, 18 (2007), pp. 221–251.
[9] H. W. Broer, V. Naudot, R. Roussarie, K. Saleh, and F. O. O. Wagener, *Organizing centers in the semi-global analysis of dynamical systems*, Int. J. Appl. Math. Stat., 12 (2007), pp. 7–36.
[10] L. Cai, G. Chen, and D. Xiao, *Multiparametric bifurcations of an epidemiological model with strong Allee effect*, J. Math. Biol., 67 (2013), pp. 185–215.
[11] S. Chow, C. Li, and D. Wang, *Normal Forms and Bifurcation of Planar Vector Fields*, Cambridge University Press, Cambridge, 1994.
[12] F. Dumortier, P. Fiddelaers, and C. Li, *Generic unfolding of the nilpotent saddle of codimension four*, in Global Analysis of Dynamical Systems, Institute of Physics, Bristol, England, 2001, pp. 131–166.
[13] F. Dumortier, R. Roussarie, and J. Sotomayor, *Generic* 3*-parameter families of vector fields on the plane, unfolding a singularity with nilpotent linear part. The cusp case of codimension* 3, Ergodic Theory Dynam. Systems, 7 (1987), pp. 375–413.
[14] F. Dumortier and C. Rousseau, *Cubic Liénard equations with linear damping*, Nonlinearity, 3 (1990), pp. 1015–1039.
[15] F. Dumortier, R. Roussarie, J. Sotomayor, and K. Zoladek, *Bifurcation of Planar Vector Fields, Nilpotent Singularities and Abelian Integrals*, Lecture Notes in Math. 1480, Springer, Berlin, 1991.
[16] A. Erbach, F. Lutscher, and G. Seo, *Bistability and limit cycles in generalist predator-prey dynamics*, Ecol. Complex., 14 (2013), pp. 48–55.
[17] I. Gelfand, M. Kapranov, and A. Zelevinsky, *Resultants and Multidimensional Determinants*, Birkhäuser, Boston, 1994.
[18] G. Dangelmayr and J. Guckenheimer, *On a four parameter family of planar vector fields*, Arch. Ration. Mech. Anal., 97 (1987), pp. 321–352.
[19] A. Hastings, K. Abbott, K. Cuddington, T. Francis, G. Gellner, Y.-C. Lai, A. Morozov, S. Petrovskii, K. Scranton, and M. L. Zeeman, *Transient phenomena in ecology*, Science, 361 (2018), eaat6412.
[20] A. I. Khibnik, B. Krauskopf, and C. Rousseau, *Global study of a family of cubic Liénard equations*, Nonlinearity, 11 (1998), 1505.
[21] C. Li and C. Rousseau, *A system with three limit cycles appearing in a Hopf bifurcation and dying in a homoclinic bifurcation: The cusp of order* 4, J. Differential Equations, 79 (1989), pp. 132–167.
[22] S. Laurin and C. Rousseau, *Organizing center for the bifurcation analysis of a generalized Gause model with prey harvesting and Holling response function of type* III, J. Differential Equations, 251 (2011), pp. 2980–2986.
[23] A. J. Lotka, *Elements of Physical Biology*, Williams and Wilkins, Baltimore, 1925.
[24] M. Lu and J. Huang, *Global analysis in Bazykin's model with Holling* II *functional response and predator competition*, J. Differential. Equations, 280 (2021), pp. 99–138.
[25] M. Lu, J. Huang, S. Ruan, and P. Yu, *Bifurcation analysis of an SIRS epidemic model with a generalized nonmonotone and saturated incidence rate*, J. Differential Equations, 267 (2019), pp. 1859–1898.
[26] R. M. May, *Simple mathematical models with very complicated dynamics*, Nature, 261 (1976), pp. 459–467.
[27] A. Morozov, K. Abbott, K. Cuddington, T. Francis, G. Gellner, A. Hastings, Y.-C. Lai, S. Petrovskii, K. Scranton, and M. L. Zeeman, *Long transients in ecology: Theory and applications*, Phys. Life Rev., 32 (2020), pp. 1–40.
[28] D. Sen, S. Ghorai, S. Sharma, and M. Banerjee, *Allee effect in prey's growth reduces the dynamical complexity in prey-predator model with generalist predator*, Appl. Math. Model., 91 (2021), pp. 768–790.
[29] M. L. Rosenzweig and R. MacArthur, *Graphical representation and stability conditions of predator-prey interactions*, Amer. Nat., 97 (1963), pp. 209–223.

[30] M. L. Rosenzweig, *Paradox of enrichment: Destabilization of exploitation ecosystems in ecological time*, Science, 171 (1971), pp. 385–387.
[31] F. Takens, *Forced oscillations and bifurcation*, in Applications of Global Analysis I, Commun. Math. Insti. Rijksuniversiteit Utrecht 3, 1974, pp. 1–59.
[32] V. Volterra, *Fluctuations in the abundance of species considered mathematically*, Nature, 118 (1926), pp. 558–560.
[33] C. Xiang, J. Huang, S. Ruan, and D. Xiao, *Bifurcation analysis in a host-generalist parasitoid model with Holling* II *functional response*, J. Differential Equations, 268 (2020), pp. 4618–4662.
[34] C. Xiang, J. Huang, and H. Wang, *Linking bifurcation analysis of Holling-Tanner model with generalist predator to a changing environment*, Stud. Appl. Math., 149 (2022), pp. 124–163.
[35] C. Xiang, M. Lu, and J. Huang, *Degenerate Bogdanov-Takens bifurcation of codimension* 4 *in Holling-Tanner model with harvesting*, J. Differential Equations, 314 (2022), pp. 370–417.
[36] D. Xiao, *Bifurcations of saddle singularity of codimension three of a planar vector field with nilpotent linear part*, Sci. Sin. A, 23 (1993), pp. 252–260.
[37] D. Xiao, *Bifurcations on a five-parameter family of planar vector field*, J. Dynam. Differential Equations, 20 (2008), pp. 961–980.
[38] D. Xiao and F. Zhang, *Multiple bifurcations of a predator-prey system*, Discrete Contin. Dyn. Syst. Ser. B, 8 (2007), pp. 417–437.
[39] L. Yang, *Recent advances on determining the number of real roots of parametric polynomials*, J. Symbolic Comput., 28 (1999), pp. 225–242.
[40] P. Yuan, L. Chen, M. You, and H. Zhu, *Dynamics complexity of generalist predatory mite and the leafhopper pest in tea plantations*, J. Dynam. Differential Equations, https://doi.org/10.1007/s10884-021-10079-1 (2021).
[41] Z. Zhang, T. Ding, W. Huang, and Z. Dong, *Qualitative Theory of Differential Equations*, Transl. Math. Monogr. 101, American Mathematical Society, Providence, RI, 1992.
[42] H. Zhu, S. A. Campbell, and G. S. K. Wolkowicz, *Bifurcation analysis of a predator-prey system with nonmonotonic functional response*, SIAM J. Appl. Math., 63 (2003), pp. 636–682.
[43] H. Zhu and C. Rousseau, *Finite cyclicity of graphics with nilpotent singularity of saddle or elliptic type*, J. Differential Equations, 178 (2002), pp. 325–436.